ACS Infectious Diseases

Article

Biosynthesis, Mechanism of Action, and Inhibition of the Enterotoxin Tilimycin Produced by the Opportunistic Pathogen Klebsiella oxytoca

Evan M. Alexander, Dale F. Kreitler, Valeria Guidolin, Alexander K Hurben, Eric J Drake, Peter W. Villalta, Silvia Balbo, Andrew M. Gulick, and Courtney C. Aldrich

ACS Infect. Dis., **Just Accepted Manuscript** • DOI: 10.1021/acsinfecdis.0c00326 • Publication Date (Web): 02 Jun 2020

Just Accepted

is published by the American Chemical Society. 1155 Sixteenth Street N.W., Washington, DC 20036

Biosynthesis, Mechanism of Action, and Inhibition of the Enterotoxin Tilimycin Produced by the Opportunistic Pathogen *Klebsiella oxytoca*

Evan M. Alexander,[1] Dale F. Kreitler,[2] Valeria Guidolin,[3,4] Alexander K. Hurben,[1] Eric Drake,[2] Peter W. Villalta,[1,3] Silvia Balbo,[3,4*] Andrew M. Gulick,[2*] Courtney C. Aldrich[1*]

[1]Department of Medicinal Chemistry, University of Minnesota, Minneapolis, MN, 55455, USA

[2] Department of Structural Biology, Jacobs School of Medicine and Biomedical Sciences University at Buffalo, Buffalo, New York 14203, USA

[3]Masonic Cancer Center, University of Minnesota, Minneapolis, MN, 55455, USA

[4]Division of Environmental Health Sciences, School of Public Health, University of Minnesota, Minneapolis, MN, 55455, USA

KEYWORDS: Nonribosomal peptide synthetase, adenylation, microbiome, tilimycin, pyrrolobenzodiazepine, *Klebsiella oxytoca*

ABSTRACT

Tilimycin is an enterotoxin produced by the opportunistic pathogen *Klebsiella oxytoca* that causes antibiotic-associated hemorrhagic colitis (AAHC). This pyrrolobenzodiazepine (PBD) natural product is synthesized by a bimodular nonribosomal peptide synthetase (NRPS) pathway comprised of three proteins: NpsA, ThdA and NpsB. We describe the functional and structural characterization of the fully reconstituted NRPS system and report the steady-state kinetic analysis of all natural substrates and cofactors as well as the structural characterization of both NpsA and ThdA. The mechanism of action of tilimycin was confirmed using DNA adductomics techniques through the detection of putative N-2 guanine alkylation after tilimycin exposure to eukaryotic cells, providing the first structural characterization of a PBD-DNA adduct formed in cells. Finally, we report the rational design of small-molecule inhibitors that block tilimycin biosynthesis in whole cell *K. oxytoca* (IC_{50} = 29 ± 4 μM) through the inhibition of NpsA (K_D = 29 ± 4 nM).

INTRODUCTION

The gastrointestinal (GI) tract of every human houses an extraordinarily complex ecosystem of microorganisms, collectively known as the GI microbiota, with representation of over one thousand different species from all domains of life.[1] Advances in metagenomic screening over the past decade have begun to reveal the profound influence of the GI microbiota on human health and disease.[2–7] Normally, these commensal microorganisms work harmoniously with the human host to maintain a symbiotic relationship,[8,9] but disturbance of the gut microbiota leads to dysbiosis, which can have far reaching effects.[10,11] While many chronic diseases including inflammatory bowel disease, obesity, diabetes, and neurodegenerative disorders have been correlated to dysbiosis of gut microbial communities,[12–22] the causative links between microbiota and disease are often shrouded by the complexity of the host-microbiota interactions.

Klebsiella oxytoca and its role in antibiotic-associated hemorrhagic colitis (AAHC) serves as a model for understanding the molecular basis of a disease caused by an imbalance of the gut microbiota.[23–25] *K. oxytoca* is an opportunistic gram-negative bacterial species that resides at low abundance in the colon of 2–10 percent of healthy individuals.[23,26] Following β-lactam antibiotic treatment, *K. oxytoca* utilizes its constitutively expressed β-lactamase to survive while commensal bacteria are eliminated. In the absence of an otherwise competitive microbial community, *K. oxytoca* thrives, triggering severe dysbiosis. Subsequent expansion of *K. oxytoca* in the colon leads to overproduction of tilivalline and related small molecule enterotoxins that cause apoptosis of colonic epithelium cells.[27–30] Originally, the cytotoxicity and corresponding AAHC was attributed solely to tilivalline,[23,31,32] but further analysis led to the identification of tilimycin,[27–29] which is a more potent cytotoxin and likely plays a greater role in the pathogenicity of *K. oxytoca*.[30,33]

Tilimycin is a tricyclic pyrrolobenzodiazepine synthesized by *K. oxytoca* via a nonribosomal peptide synthetase (NRPS) pathway (**Figure 1**).[24,28,29] NRPSs are large multi-modular proteins responsible for the synthesis of short peptides in an assembly line like fashion, independent of mRNA ribosomal machinery. The formation of a single amide bond in a NRPS module requires three unique domains. First, an adenylation domain (A) is responsible for amino acid selection, activation and transfer onto the downstream thiolation domain. The thiolation domain (T) contains a flexible and mobile phosphopantetheinyl cofactor arm which carries the amino acid that is connected via a thioester linkage. Finally, a condensation domain (C) catalyzes amide bond formation between two loaded amino acids.[34] Tilimycin biosynthesis is performed by a bimodular NRPS comprised of NpsA, ThdA and NpsB. NpsA and ThdA are stand-alone proteins for adenylation and thiolation respectively while NpsB contains a complete C-A-T module along with a C-terminal reductase (Re) domain for release of tilimycin. Bioinformatic analyses of signature sequences within the adenylation domains suggest 3-hydroxyanthranilic acid is the substrate for NpsA while NpsB confers specificity for L-proline.[24] Thus, NpsA is predicted to activate and load the stand alone thiolation protein ThdA with 3-hydroxyanthranilic acid, while NpsB activates and loads L-proline on to its corresponding thiolation domain. The condensation domain is predicted to catalyze amide bond formation between the 3-hydroxyanthranilate thioester and the free amine of L-proline to afford the L-*N*-(3-hydroxyanthraniloyl)prolyl-S~T_{NpsB} acyl-peptide intermediate followed by reductive release of the thioester to L-*N*-(3-hydroxyanthraniloyl)prolinal mediated by the reductase domain.[24] Ring-chain tautomerization of the amino aldehyde to the close-chain hemiaminals yields tilimycin. which can undergo non-enzymatic reaction with indole, produced in large quantities endogenously in *K. oxytoca*, to afford tilivalline.[33]

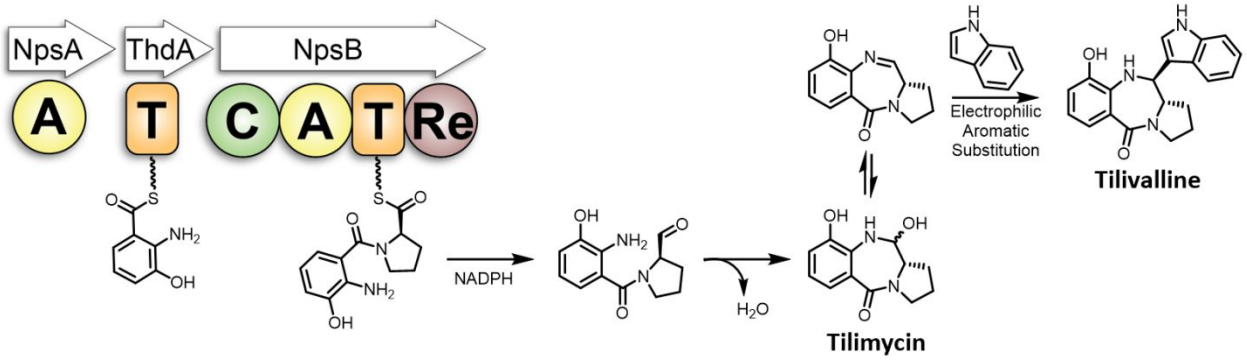

Figure 1. The NRPS pathway for the biosynthesis of tilimycin. Reductive release of the dipeptide affords L-*N*-(3-hydroxyanthraniloyl)prolinal that spontaneously cyclizes to a mixture of diastereomeric aminals known as tilimycin that are in equilibrium with the imine species. Non-enzymatic condensation with indole yields tilivalline. A = adenylation domain, T = thiolation domain, C = condensation domain, Re = thioester-reductase domain.

Herein we report the detailed functional and structural characterization of the tilimycin biosynthetic pathway that extends prior metabolic profiling and mutasynthesis studies to define the overall pathway and substrate tolerance.[28] We then describe the synthesis of two classes of rationally designed bisubstrate inhibitors which enabled structural characterization of NpsA and a NpsA-ThdA fusion protein in the adenylation and thioester conformations, respectively. One of the bisubstrate inhibitors was shown to selectively inhibit tilimycin synthesis in cell culture without impairing bacterial replication. Finally, to investigate the molecular mechanism of action of the pyrrolobenzodiazepine class of natural products, we utilized DNA adductomic techniques to successfully detect and structurally characterize alkylated DNA from eukaryotic cells exposed to tilimycin, helping to further clarify the causative link between a microbiota derived natural product and human disease.

RESULTS

Cloning, Expression and Purification of NpsA, *holo*-ThdA and *holo*-NpsB. The *thdA* and *npsB* genes were PCR amplified from *K. oxytoca* strain MIT-5243 genomic DNA and cloned

into a pET15b vector containing a TEV cleavage site and a 5-His affinity tag at the N-terminus. The *npsA* gene was codon optimized for expression in *E. coli*, synthesized and cloned into a pET15b vector containing an identical 5-His TEV cleavage site. The plasmids were transformed and overexpressed in *E. coli* BL21(DE3) cells. Two step purification was performed starting with immobilized metal affinity chromatography (IMAC). The partially purified *apo*-ThdA and *apo*-NpsB were incubated with the promiscuous phosphopantetheinyl transferase Sfp from *Bacillus subtilis* to ensure conversion to the *holo* protein form. Subsequent size exclusion chromatography afforded 20 mg/L of NpsA, 27 mg/L of *holo*-ThdA and 3 mg/L of *holo*-NpsB. The molecular mass of the proteins determined by SDS-PAGE were consistent with their calculated molecular weight: ~56 kDa (55,772 kDa calculated) for NpsA, ~10 kDa (9,486 kDa calculated) for *holo*-ThdA, and ~150 kDa (164,015 kDa calculated) for *holo*-NpsB (**Figure S1**).

Biochemical Characterization of NpsA and ThdA. NpsA catalyzes a two-step ATP-dependent acylation of the phosphopantetheine prosthetic group of *holo*-ThdA to yield 3-hydroxyanthraniloyl-ThdA (*acyl*-ThdA) that proceeds through a 3-hydroxyanthraniloyl adenosine monophosphate (3HA-AMP) intermediate (**Figure 2A**). Catalysis of these two steps requires dynamic movement of the C-terminal hinge region of NpsA as observed in other adenylating enzymes.[35–37] Initially, the "closed" adenylation conformation allows for binding and ligation of aryl-acid and ATP substrates. The "open" thiolation conformation enables *holo*-ThdA recruitment and subsequent acylation. While prior *in vitro* mutasynthesis studies have revealed that NpsA possesses relaxed substrate specificity for anthranilic acid derivatives[27–29], steady-state kinetic characterization of NpsA has not been reported. To assess the steady-state kinetics of the complete adenylation-acylation reaction, we used a continuous coupled assay wherein the pyrophosphate (PPi) byproduct generated in the initial adenylation reaction is converted to

phosphate by inorganic pyrophosphatase and then purine nucleoside phosphorylase catalyzes the phosphorolysis of 7-methylthioguanosine to 7-methylthioguanine (MesG), whose formation can be monitored at 360 nm.[38,39] We confirmed the reaction velocity was linearly dependent on NpsA concentration for this coupled assay. ThdA was also required for full activity and the reaction rate decreased 140-fold in the absence of ThdA. Initial velocity experiments were performed by varying one substrate at fixed saturating concentrations of the other two substrates and provided apparent K_M values of 63, 15 and 3.4 μM for 3-hydroxyanthranilic acid, ATP and *holo*-ThdA, respectively, with an average apparent k_{cat} equal to 0.89 s^{-1} (**Figure 2A, Table 1**). Because of reduced rates at high concentrations of ThdA, the kinetic data were fit to a substrate-inhibited model providing a substrate inhibition constant, K_i of 15 μM. Interestingly, substrate inhibition by thiolation domains has not been previously observed. We next explored the substrate specificity of 3-hydroxyanthranilic acid with 3-hydroxybenzoic acid and anthranilic acid to probe the importance of the 2-amino or 3-hydroxyl substituents. Removal of the 3-hydroxy group in anthranilic acid led to a 52-fold decrease in the specificity constant (k_{cat}/K_M), while deletion of the 2-amino group in 3-hydroxybenzoic acid provided a more pronounced 200-fold decrease in specificity constant indicating the 2-amino group is more critical for catalytic efficiency than the 3-hydroxy group.

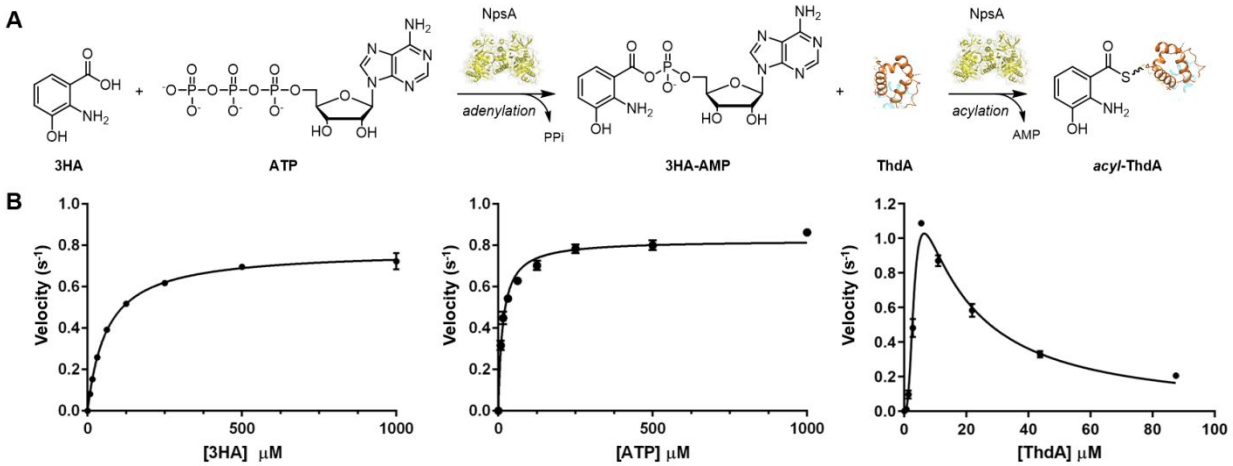

Figure 2: A) Adenylation-ligation enzymatic reaction catalyzed by NpsA. B) Initial velocity vs substrate concentration [3HA], [ATP] and [ThdA]. Data were fit to the Michaelis-Menten equation or substrate inhibition model. Each reaction contained 5 mM ATP and 20 μM ThdA (for varying 3HA), 500 μM 3-HA and 20 μM ThdA (for varying 3-ATP), 500 μM 3HA and 5 mM ATP (for varying ThdA) in 50 mM Tris, 150 mM NaCl, 10 mM $MgCl_2$ pH 8 buffer with 20 nM NpsA. Data are average (±SD) of triplicate experiments.

Table 1. Apparent Kinetic parameters for NpsA.

Substrate	K_M (μM)	k_{cat} (s^{-1})	k_{cat}/K_M ($M^{-1}\cdot s^{-1}$)
3-Hydroxyanthranilic acid	$(6.3 \pm 0.2) \times 10^1$	0.78 ± 0.01	$(1.8 \pm 0.1) \times 10^4$
3-Hydroxybenzoic acid	$(4.0 \pm 0.9) \times 10^3$	0.35 ± 0.07	$(8.8 \pm 2.6) \times 10^1$
Anthranilic acid	$(8.5 \pm 0.7) \times 10^2$	0.29 ± 0.01	$(3.4 \pm 0.3) \times 10^2$
ATP	$(1.5 \pm 0.1) \times 10^1$	0.82 ± 0.01	$(5.6 \pm 0.4) \times 10^4$
holo-ThdA	3.4 ± 0.2, ($K_i = 15 \pm 2$)	1.08 ± 0.02	$(3.2 \pm 0.2) \times 10^5$

Characterization of NpsB and Fully Reconstituted Assay. The next downstream enzyme in the NRPS pathway is NpsB with a C-A-T-Re multidomain architecture. Unlike the stand-alone proteins NpsA and ThdA, the enzymatic activities of NpsB cannot be easily decoupled. We initially attempted to interrogate the activity of the embedded adenylation domain of NpsB employing hydroxylamine to facilitate enzyme turnover by reaction with the acyl-adenylate intermediate using the coupled assay employed for NpsA.[40,41] Addition of hydroxylamine to the

NpsB assay containing saturating L-proline and ATP did not stimulate enzyme turnover as measured by PPi release suggesting acyl transfer to the prolyl-loaded thiolation domain (L-Pro-S~T_{NpsB}) was rapid or the initial L-Pro-adenylate was inaccessible for reaction with hydroxylamine (**Figure S2**). The observed steady-state rate for PPi formation of 0.01 sec^{-1} (that is dependent on both L-proline and ATP) is consistent with the leak of the acyl-adenylate from the adenylation domain, which enables slow enzyme turnover. We next explored whether addition of NADPH to the NpsB assay containing saturating L-proline and ATP could induce turnover of L-prolyl-S~T_{NpsB} through reduction of the proline thioester by the reductase (Re) domain to a prolinal shunt product (**Figure 3A,** red arrow). However, addition of NADPH did not stimulate enzyme turnover as measured by PPi release or NADPH consumption which suggests the Re domain is only operative on the native L-*N*-(3-hydroxyanthraniloyl)prolyl-S~T_{NpsB} substrate. To test this hypothesis, we developed a fully reconstituted assay with stoichiometric 3-hydroxyanthraniloyl-S~ThdA as substrate, which could be generated by pre-incubating stoichiometric ThdA with catalytic NpsA and 3-hydroxyanthranilic acid. Incubation of the substrates 3-hydroxyanthraniloyl-S~ThdA, L-proline, ATP and NADPH with catalytic NpsB afforded tilimycin as confirmed with an authentic synthetic standard (**Figure 3A**, blue arrow). To investigate the apparent steady-state enzyme kinetic parameters of NpsB, we measured NADPH consumption at 340 nm and varied the concentration of one substrate (i.e. L-proline) at fixed saturating concentration of the other two substrates (i.e. ATP and NADPH) along with 20 μM 3-hydroxyanthraniloyl-S~ThdA. Initial velocity experiments provided apparent K_M values of 1.8×10^3, 21 and 57 μM for of L-proline, ATP and NADPH, respectively with an average apparent k_{cat} equal to 0.050 s^{-1} (**Figure 3B, Table 2**)

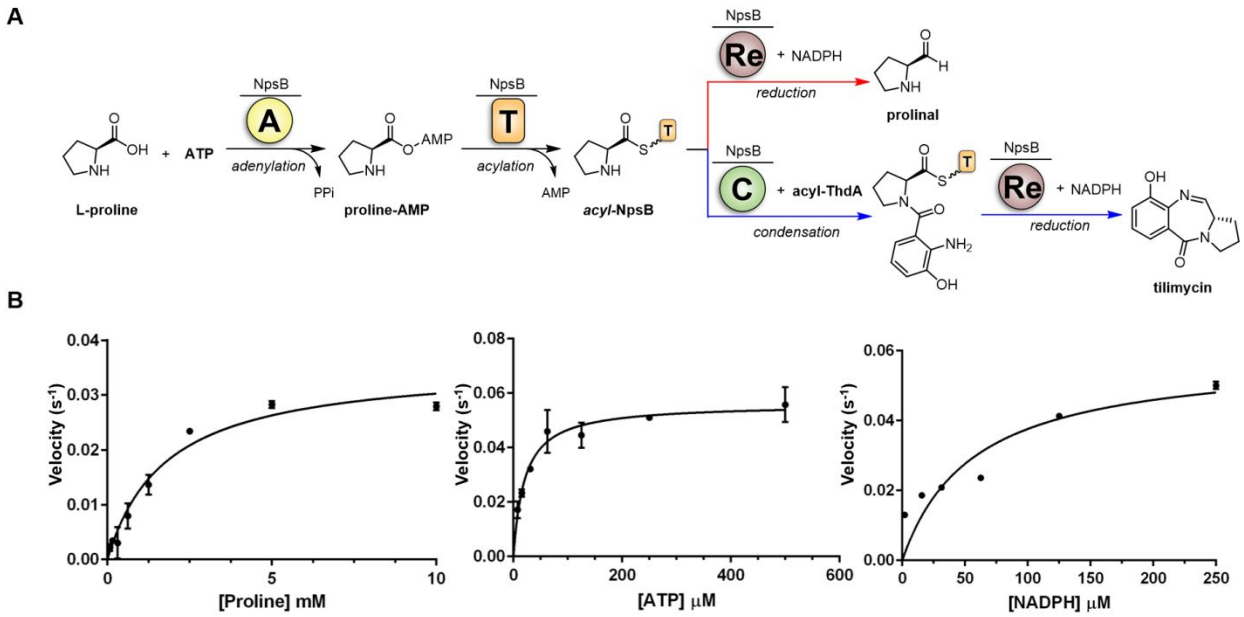

Figure 3. A) Overall enzymatic reaction catalyzed by NpsB. The A-domain of NpsB activates L-proline to the prolyl-adenylate species and transfers it to the downstream T-domain of NpsB. The intermediate L-Pro-S~T can undergo two competitive reactions: direct reduction by the reductase domain (red arrow) or condensation with *acyl*-ThdA (blue arrow), which can subsequently be reduced by the Re domain to afford tilimycin. B) Initial velocity vs substrate concentration [L-Proline], [ATP] and [NADPH]. Data were fit to the Michaelis-Menten equation. Each reaction contained 5 mM ATP and 0.5 mM NADPH (for varying L-Proline), 5 mM L-Proline and 0.5 mM NADPH (for varying ATP), 5 mM L-Proline and 5 mM ATP (for varying NADPH) in 50 mM Tris, 150 mM NaCl, 10 mM $MgCl_2$ pH 8 buffer with 250 nM NpsB and 20 μM 3-hydroxyanthraniloyl-S~ThdA. Data are average (±SD) of triplicate experiments.

Table 2. Apparent Kinetic parameters for NpsB.

Substrate	K_M (μM)	k_{cat} (s^{-1})	k_{cat}/K_M ($M^{-1}\cdot s^{-1}$)
L-Proline	$(1.8 \pm 0.3) \times 10^3$	0.037 ± 0.002	$(2.1 \pm 0.4) \times 10^1$
ATP	$(2.1 \pm 0.3) \times 10^1$	0.056 ± 0.002	$(2.7 \pm 0.4) \times 10^3$
NADPH	$(5.7 \pm 1.7) \times 10^1$	0.058 ± 0.007	$(1.0 \pm 0.3) \times 10^3$

Rational Design and Synthesis of NpsA Inhibitors. Adenylation enzyme inhibitors that mimic the acyl-AMP intermediate (**Figure 4A** and **4B**) can be developed by replacing the labile phosphate moiety of the acyl-AMP with a stabile non-cleavable bioisostere such as sulfamide to afford an acyl adenosine monosulfamide (acyl-AMS) inhibitor.[42] The sulfamide moiety closely

mimics the tetrahedral geometry and charge distribution of the ionized phosphate group, but is chemically and enzymatically stabile. Acyl-AMS inhibitors derive their high affinity by simultaneously interacting with the carboxylic acid and ATP binding pockets of the adenylation domain while their specificity arises from the acyl group. The NRPS assembly line responsible for tilimycin biosynthesis contains two potential adenylation domain targets, NpsA and NpsB. The stand-alone adenylating enzyme NpsA was selected as a target because it uses the esoteric substrate, 3-hydroxyanthranilic acid, ensuring higher selectivity than NpsB, whose adenylation domain is functionally related to prolyl tRNA synthetases found in all domains of life.[43]

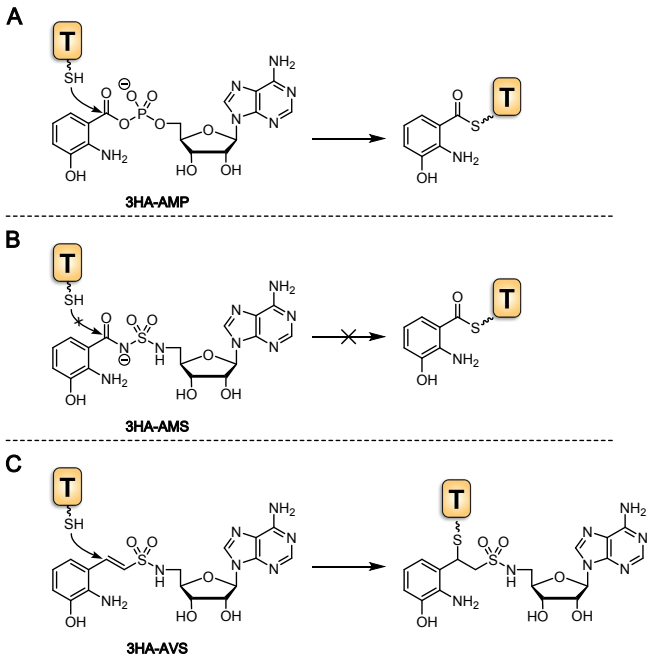

Figure 4. A) The mechanism in which 3-hydroxyanthraniloyl-adenylate is loaded to the *holo*-ThdA phosphopantetheinyl arm yielding *acyl*-ThdA. B) Non-cleavable bioisostere 3-hydroxyanthraniloyl-AMS mimicking the adenylate intermediate, inhibiting acylation of the downstream ThdA. C.) Vinyl-sulfonamide 3-hydroxyanthraniloyl-AVS participates in a hetero-Michael addition with the terminal phosphopantetheinyl thiol of *holo*-ThdA resulting in covalent modification and irreversible inhibition.

Based on the above considerations, we designed the inhibitor 3-hydroxyanthraniloyl-AMS **5**. The synthesis commenced from 2′,3′-isopropylideneadenosine **1** that was converted to the 5′-

azido nucleoside **2**[44] followed by catalytic hydrogenation to the intermediate amino derivative, which was directly condensed with sulfamide using our recently developed method by refluxing in 1,4-dioxane to afford **3** (**Scheme 1A**).[45] Acylation of **3** with *N*-hydroxysuccinimidyl (NHS) ester **7** promoted by Cs_2CO_3 in DMF furnished acyl-sulfamide **4**. Catalytic hydrogenolysis of the 3-benzyloxy ether and concomitant reduction of the 2-nitro group using Pd/C in methanol followed by TFA deprotection of the acetonide afforded the final product 3-hydroxyanthraniloyl-AMS **5** in a 45% overall yield after purification by preparative reverse-phase high-performance liquid chromatography (HPLC). The *N*-hydroxysuccinimidyl ester **7** was synthesized from the 3-benzyloxy-2-nitrobenzoic acid **6**[46] by DCC-mediated coupling with *N*-hydroxysuccinimide (**Scheme 1B**). To explore the SAR of 3-hydroxyanthraniloyl-AMS **5**, we also prepared two closely related analogues, 3-hydroxybenzoyl-AMS **8** and anthraniloyl-AMS **9** through deletion of the 2-amino and 3-hydroxy functional groups present in the aryl acid moiety (**Scheme 1C**). These were prepared analogously to **5** as described in the Supporting Information starting from 2-anthranilic acid and 3-hydroxybenzoic acid.

Scheme 1. Synthesis of 3-hydroxyanthraniloyl-AMS (**5**).

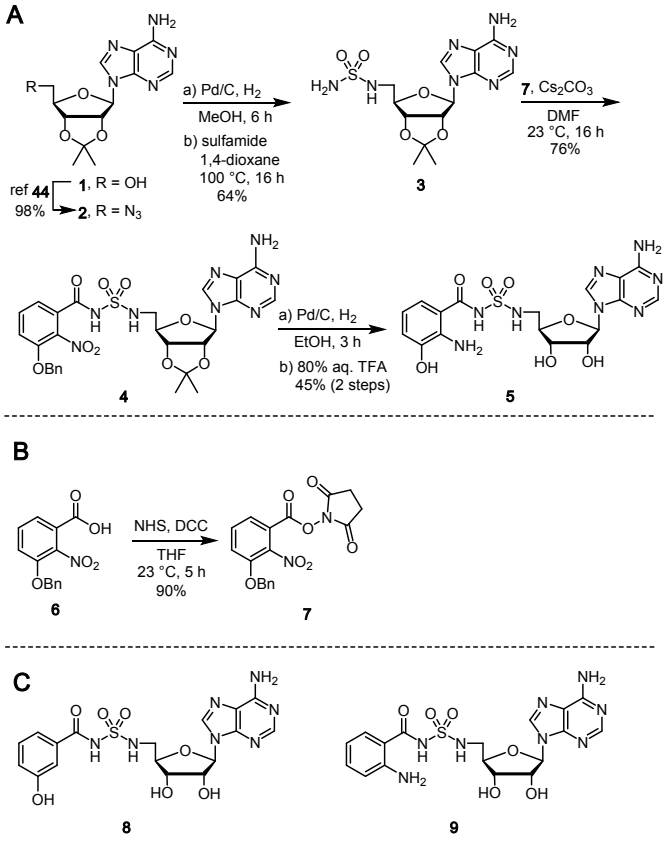

We next synthesized a second class of adenylation inhibitor that incorporates a vinylsulfonamide isostere of the acyl-phosphate linkage.[47,48] Adenosine vinylsulfonamide (AVS) inhibitors mimic the acyl-adenylate intermediate, but contain a reactive Michael acceptor at the precise position of the incoming phosphopantetheine thiol that irreversibly binds the downstream thiolation domain. AVS inhibitors thus cross-link the adenylation and thiolation domains, stabilizing their transient interaction and are useful for capturing the adenylation domain in the thioester conformation (**Figure 4C**).[49,50]

We designed 3-hydroxybenzoyl-AVS **13** for structural characterization of NpsA in complex with ThdA. Notably, **13** lacks a 2-amino group on the aryl ring due to the oxidative instability of the *ortho*-aminophenol moiety observed under the extended crystallization trials. The 3-hydroxy

group was retained since it is more important for NpsA binding (*vide infra*). Synthesis of ligand **13** was achieved in three steps beginning with Horner-Wittig condensation of 3-hydroxybenzaldehyde **10** and *N*-Boc-diphenylphosphoryl sulfonamide[51] to afford *E*-vinylsulfonamide **11** (**Scheme 2**). Subsequent Mitsunobu coupling of **11** with 2′,3′-isopropylideneadenosine **1** gave **12**. Global deprotection of the MOM, Boc and acetonide groups using TFA yielded the final 3-hydroxybenzoyl-AVS **13**.

Scheme 2. Synthesis of 3-hydroxybenzoyl-AVS (**13**).

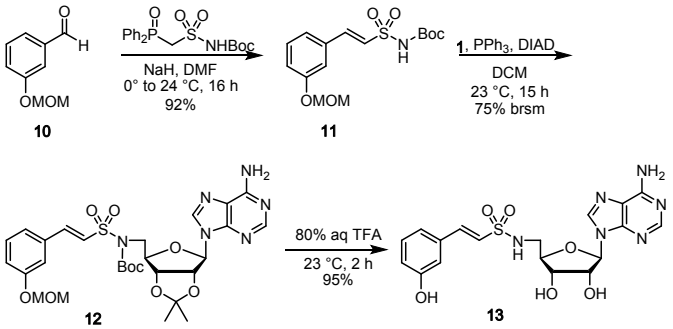

Biophysical and Biochemical Characterization of AMS inhibitors. Acyl-adenylate inhibitors **5**, **8**, and **9** were evaluated for enzyme inhibition of NpsA using our coupled assay with 20 nM NpsA and 20 μM ThdA under initial velocity conditions in the presence of saturating concentrations of 3-hydroxyanthranilic acid (500 μM) and ATP (5 mM). The concentration-response plots were fit to the Morrison equation for tight binding inhibition to determine the inhibition constants (**Figure 5A**). The lead inhibitor 3-hydroxylanthraniloyl-AMS **5** exhibited an $appK_i$ = 54 nM (**Table 3**). Analog **8** lacking the 2-amino group had a modest 4-fold loss of potency while analog **9** devoid of the 3-hydroxyl group was 22-fold less potent than **5**.

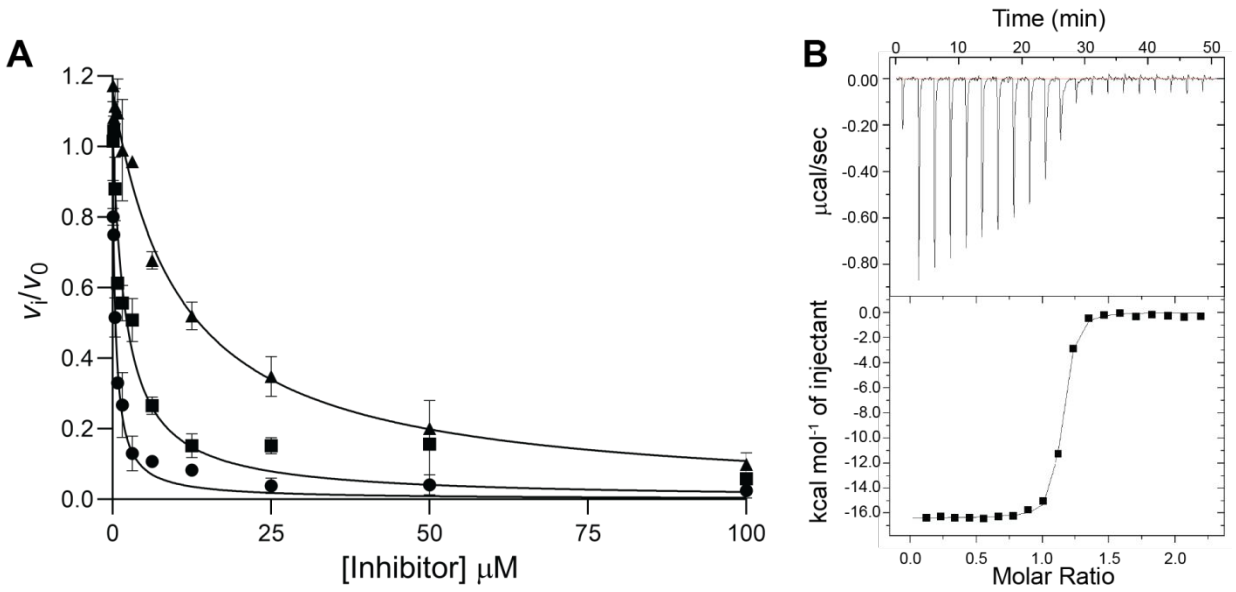

Figure 5. A) Concentration-response plot for NpsA inhibition by **5**, **8** and **9**: 3-hydroxyanthraniloyl-AMS **5** (circle), 3-hydroxybenzoyl-AMS **8** (square), anthraniloyl-AMS **9** (triangle). The curve represents the best non-linear fit to the Morrison equation. Data are average (±SD) of triplicate experiments. B) Representative ITC binding isotherm of binding **5** to NpsA. (Top) Data obtained by titration of 25 nM NpsA with 0.25 μM **5**. (Bottom) The integrated curve showing experimental points and the best fit (–).

Table 3: Summary of characterization of all three inhibitors against purified NpsA.

Cmpd	appK_i (nM)	K_D (nM)	ΔH (kcal/mol)	TΔS (kcal/mol)	ΔG (kcal/mol)	n
5	$(5.4 \pm 0.8) \times 10^1$	$(2.93 \pm 0.28) \times 10^1$	$(-1.61 \pm 0.16) \times 10^1$	-5.67 ± 0.21	$(1.04 \pm 0.16) \times 10^1$	1.06 ± 0.03
8	$(2.3 \pm 0.4) \times 10^2$	$(1.12 \pm 0.68) \times 10^2$	$(-1.64 \pm 0.29) \times 10^1$	-6.92 ± 2.91	9.45 ± 0.23	0.94 ± 0.01
9	$(1.2 \pm 0.1) \times 10^3$	$(4.85 \pm 2.50) \times 10^2$	$(-1.09 \pm 0.35) \times 10^1$	-2.31 ± 0.47	8.59 ± 0.31	1.17 ±0 .02

We also determined the binding affinities of **5**, **8** and **9** to NpsA by isothermal titration calorimetry to provide the dissociation constant (K_D), Gibbs free energy (ΔG), enthalpy (ΔH), and entropy (ΔS) of the protein-ligand interactions (**Table 3, Figure 5B**). Compound **5** binds tightly with a K_D of 29 nM, a value in close agreement to the apparent K_i value of 54 nM

measured using the functional kinetic assay. Binding is enthalpically driven with a ΔH of -16.1 kcal/mol with a small unfavorable entropic component. Deletion of the 2-amino group in compound **8** resulted in a 4-fold decrease in K_D relative to **5** due to an increased entropic penalty, while deletion of the 3-hydroxyl in **9** provided a 17-fold decrease in K_D compared to **5** caused by a 5.5 kcal/mol loss in enthalpy that was partially compensated by an entropic gain. The relative binding affinities of **8** and **9** compared to **5** determined by ITC closely mirror the relative inhibition constants from the steady-state kinetic assay.

Structures of NpsA and ThdA. To help gain further insight into molecular interactions underpinning the observed trends in ligand affinities, we obtained an X-ray crystal structure (2.9 Å) of NpsA co-crystallized with 3-hydroxyanthraniloyl-AMS **5** (**Figure 6A**). The structure features a single chain of NpsA with 3-hydroxyanthraniloyl-AMS **5** occupying the active site and the C-terminal subdomain, A_{sub}, positioned in the adenylate forming conformation identifiable by the contact between Lys492 within the A_{sub} and the pro-*R* oxygen atom of the acyl-sulfamide.[42] The moderate resolution of this initial structure precluded unequivocal determination of the orientation of the aryl ring. Therefore, we obtained X-ray crystal structures of the NpsA N-terminal domain (in which the C-terminal subdomain of NpsA was truncated from the Asn405 hinge residue onward) in complex with compounds **5**, **8** and **9** (1.7-2.2 Å). The resolution of the 3-hydroxyanthraniloyl-AMS **5** containing structure unequivocally displays the orientation of the aryl ring suggested by the full-length structure **(Figure 6A**) in which the 3′-hydroxyl group form a tripartite H-bond with Asn207 and Ser271 (**Figure 7B**). This pose was used to deduce the orientation of the ligand in the full-length structure (**Figure 7A**). Each liganded structure features canonical nucleotide A domain interactions including: Asp388 with the ribose 2′,3′-hydroxyls; Thr298 with the pro-*S* sulfamide oxygen; Asn293 with the adenine 6-

amino group. In the aryl ring of the ligands, the 3′-hydroxy group presumably participates as an H-bond acceptor with an Asn207 donor and an H-bond donor with a Ser271 acceptor, while anthraniloyl derivatives contain the additional 2′-amino group that could potentially participate as an H-bond donor with a Ser271 acceptor.

We also generated an engineered NpsA-ThdA fusion construct and subsequently determined the 2.9 Å crystal structure of NpsA-ThdA bound to 3-hydroxybenzoyl-AVS **13** (**Figure 6B**). The final model contains four NpsA adenylation domains and four ThdA thiolation domains. The linker joining the NpsA and ThdA domains are disordered in all four chains however the termini of the respective molecules suggest that the proteins have adopted a domain swapped configuration in which the carrier domain of one protein chain is donated to a neighboring adenylation domain. This configuration was seen previously in the similar fusion construct from enterobactin biosynthesis.[48] Despite the disorder in the linker and ThdA, the interface between the adenylation and thiolation domains is consistent and is similar to the interface seen in other structures of trapped adenylation-thiolation structures.[48–50] The A_{sub} residues Arg411 and Arg414 have moved from a surface exposed loop in the adenylation conformation (**Figure 6A**) to form a clamp over the Ser542 phosphodiester and **13**, respectively in the thiolation conformation. (**Figure 6B**). The majority of the NpsA-ThdA contact is mediated by a parallel helix-helix interaction between ThdA helix 2 and a helix on the NpsA N-terminal domain that runs from Gly248 to Val257. The residue interactions between the two appear as Arg411/Arg445/Asn541 that is analogous to the Arg437/Lys473/Asp574 motif, which is conserved among the enterobactin, acinetobactin, bacillibactin and vibriobactin systems.[48]

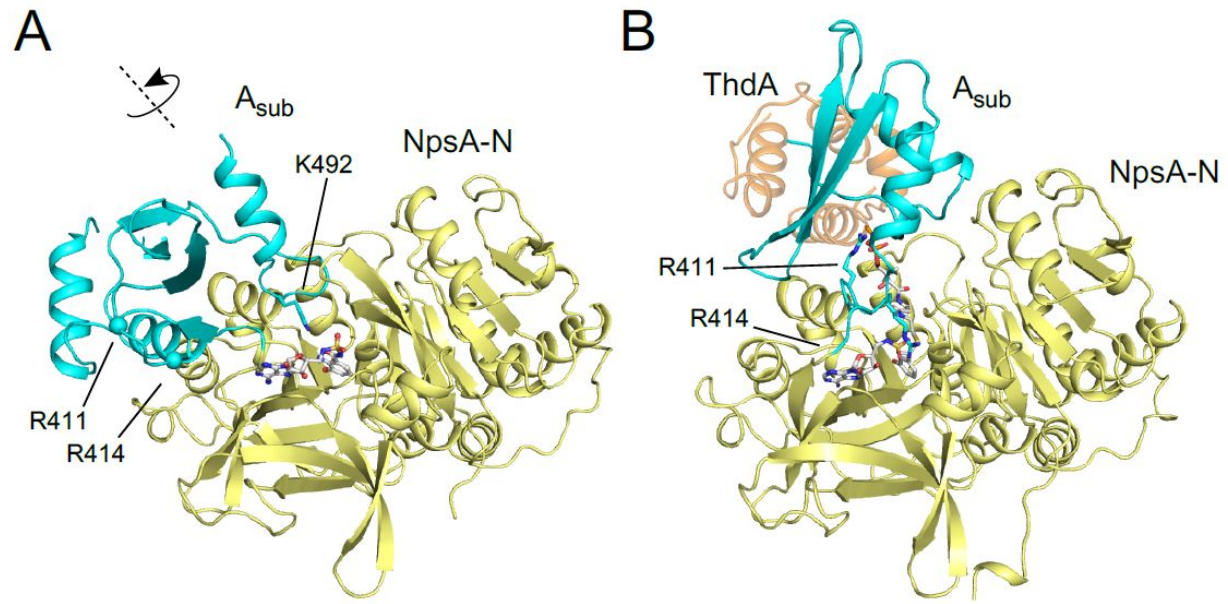

Figure 6. A) 3-hydroxyanthraniloyl-AMS **5** bound to full length NpsA showing A_{sub} domain in the adenylation conformation. B) 3-hydroxybenzoyl-AVS **13** bound to NpsA-ThdA fusion protein showing A sub domain in the acylation configuration binding auxiliary protein ThdA.

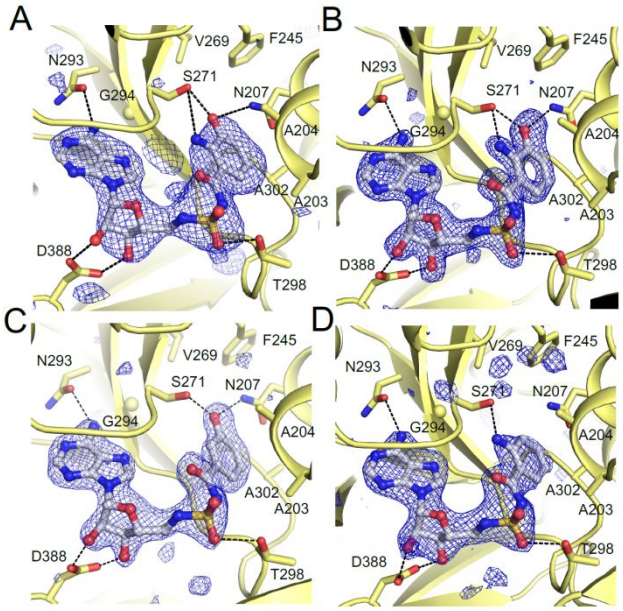

Figure 7. A) Full-length NpsA and 3-hydroxyanthraniloyl-AMS **5**, B) NpsA-N and 3-hydroxyanthraniloyl-AMS **5**, C) NpsA-N and 3-hydroxybenzoyl-AMS **8**, and D) NpsA-N and 2-anthraniloyl-AMS **9**. Each panel displays conserved A domain nucleotide binding residues (Asn293, Thr298, Asp388). Simulated annealing electron density is calculated with coefficients of the form mFo-DFc and contoured at 3σ.

Inhibition of Tilimycin Biosynthesis in *Klebsiella oxytoca.* 3-Hydroxyanthraniloyl-AMS **5** was next evaluated for its ability to inhibit tilimycin production in the clinical isolate *K. oxytoca* strain MIT 10-5243. Due to the nonenzymatic addition of indole observed in endogenous production of tilimycin, a high-performance liquid chromatography tandem mass spectrometry (LC-MS/MS) method was developed to monitor the MS^2 transition of tilivalline (334.4→199.1 *m/z)* instead. We observed tilivalline production commenced as the *K. oxytoca* culture transitioned to stationary phase at 6 hours, with peak concentrations being detected after 27 hours before declining due to degradation (**Figure S4**). We first showed 3-hydroxyanthraniloyl-AMS **5** does not inhibit growth of *K. oxytoca* at 300 μM highlighting the selectivity and nonmicrobicidal activity of this adenylation inhibitor (**Figure S5**). Tilivalline levels were subsequently measured at 8-hours following incubation of 300 μM **5**, **8**, and **9** with *K. oxytoca*. Unfortunately, inhibition of tilivalline was not detected for compound **5** and more careful examination of the growth curves revealed **5** paradoxically stimulated growth of *K. oxytoca* in earlier timepoints likely leading to the modest increase of tilivalline production observed (**Figure S5**). We speculated metabolism or degradation of **5** under the culture conditions may have been responsible for the lack of tilivalline inhibition. We quantified **5** in the culture of *K. oxytoca* during the full time course and observed 75% degradation of 3-hydroxyanthraniloyl-AMS **5** by the 8-hour timepoint (**Figure S4**). Deletion of either the 2-amino or 3-hydroxy groups of the *ortho*-aminophenol in **5** with analogs **8** and **9** was expected to abolish the potential oxidative instability and subsequent degradation. Gratifyingly, 3-hydroxybenzoyl-AMS **8** and 2-anthraniloyl-AMS **9** reduced tilivalline levels with **8** completely ablating tilivalline production under the experimental conditions (**Figure 8A**). The concentration-response plot for inhibition of

tilivalline production of the most promising inhibitor 3-hydroxybenzoyl-AMS **8** yielded an IC_{50} value of 29 μM (**Figure 8B**).

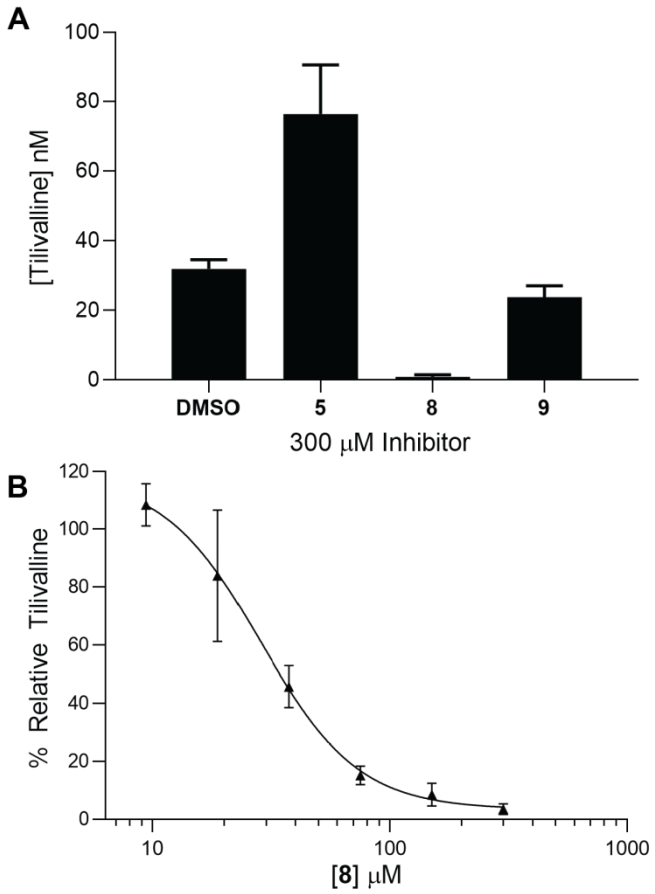

Figure 8. A) Cultures inoculated with *K. oxytoca* to a starting OD_{600} = 0.01 with 300 μM of **5, 8**, **9** or 0.6% DMSO as a negative control were grown for 8 hours at 37 °C in CASO medium shaking at 250 rpm. Tilivalline production was quantified using LC-MS/MS and the *m/z* transitions 334.4→199.1 [tilivalline (analyte)] and 424→199.1 [*O*-benzyltilivalline (internal standard)]. B) Concentration-response plot of the normalized % production of tilivalline at 8 hours under the incubation conditions described in panel A relative to a DMSO-only control versus the concentration 3-hydroxybenzoyl-AMS **8**. The curve was fit to a four-parameter Hill equation to provide an IC_{50} value of 29 ± 4 μM and a Hillslope of -2.1 ± 0.5. The data points represent the mean (±SD) of two independent experiments.

DNA Adductomics. Tilimycin belongs to a class of NRPS secondary metabolites called pyrrolobenzodiazepines.[52,53] These compounds have been observed to react *in vitro* with DNA via the electrophilic imine at the C-11 position and the nucleophilic N-2 of guanine forming a

covalent aminal bond.[54–56] Tilimycin has been predicted to react in an analogous fashion and ultimately results in single and double stranded DNA breaks.[57] Downstream effects of DNA adduct formation have been observed, however, direct detection of the DNA adducts in cells has not been observed.[33] To further verify tilimycin's mechanism of toxicity we used an LC-MS^n DNA adductomics approach to simultaneously detect both anticipated DNA adducts from direct alkylation of DNA by tilimycin, and any unanticipated DNA adducts which may form.[58] Data acquisition consists of MS and MS^2 data dependent acquisition with MS^3 fragmentation triggered upon neutral loss of 2'-deoxyribose (116.0473 *m/z*) or one of the four nucleobases (151.0494, 135.0545, 126.0429, 111.0433 *m/z*).

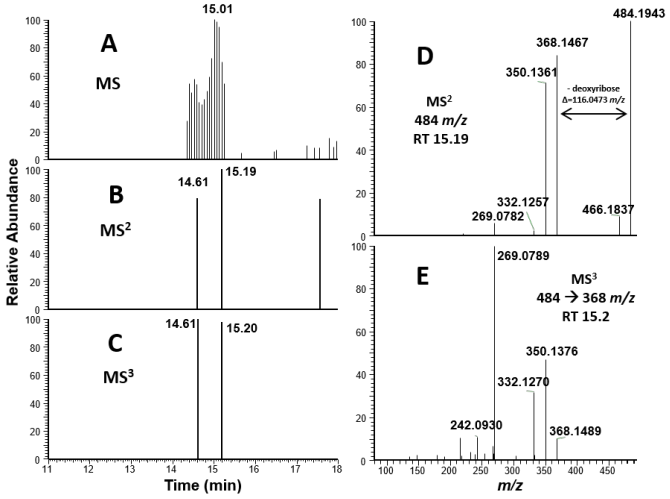

Figure 9. Mass spectral data for ctDNA treated with tilimycin. A.) MS^1 EIC of 484.1939 *m/z*. B.) MS^2 data dependent event for 484.1939 *m/z*. C.) MS^3 triggered event for 484.1939→368.1466 *m/z* (neutral loss of deoxyribose). D.) MS^2 mass spectrum from fragmentation of 484 *m/z* at retention time = 15.19 min. E.) MS^3 mass spectrum from fragmentation of 484.1939→368.1466 *m/z* at retention time = 15.20 min.

We began with exposure of either purified calf thymus DNA or ^{15}N bacterial DNA with tilimycin at 37 °C for 24 hours. The DNA was then enzymatically hydrolyzed, and the resulting mixture was purified and enriched by solid phase extraction and fractionated into three portions

(10% MeOH/H_2O, 100% MeOH, 2% formic acid/MeOH). Each fraction was analyzed to detect and identify DNA adducts which formed due to the exposure. The proposed adduct dG-tilimycin (484.1939 *m/z*) was observed in the 100% MeOH fraction with two distinct chromatographic peaks (retention times of 14.5 and 15.1 min), likely corresponding to the two diastereomers which could form upon nucleophilic addition of dG to the C-11 imine of tilimycin (**Figure 9A, Figure S6**). MS^2 fragmentation of the parent ion of dG-tilimycin (484.1939 *m/z*) resulted in the neutral loss of deoxyribose (368.1466 *m/z*) which triggered MS^3 fragmentation that was dominated by a product ion of 269.0789 *m/z* (**Figure 9E**). Confirmation of the adduct identity was aided by the ^{15}N bacterial DNA exposure which resulted in an isotopically labeled dG-tilimycin (489.1791 *m/z*; +4.9852 *m/z* for 5 ^{15}N atom incorporation in the nucleobase) with fragmentation to 373.1323 *m/z* and 274.0637 *m/z* product ions which maintain all 5 ^{15}N atoms of guanine (**Figure 10**). Along with the proposed dG-tilimycin adduct, we observed a dA-tilimycin adduct in very low abundance (**Figure S7**). In parallel, we analyzed calf thymus DNA exposed tilivalline and did not detect any adducts, consistent with the hypothesis of other laboratories that tilivalline neither degrades back into tilimycin nor interacts with DNA.

To determine if these metabolites are detectable from whole cell exposure, HEK cells were treated with 1 μM tilimycin (IC_{25}; **Figure S13**) and incubated at 37 °C for 24 hours. The cells were lysed, and the DNA was extracted, hydrolyzed, purified and enriched identically to the DNA exposure studies as describe previously. Targeted mass spectrometry of the MS^2 fragmentation of 484.1939 *m/z* yielded distinct extracted ion chromatogram (EIC) peaks of 368.1446 *m/z* (neutral loss of 2'-deoxyribose) and 350.1360 *m/z* (neutral loss of 2'-deoxyribose and H_2O) between 13.2-14.0 min (**Figure 11**) consistent with the proposed dG-tilimycin adduct

observed in the tilimycin-treated ctDNA (**Figure 9**). The dA-tilimycin adduct was not observed, likely indicating it is below the limit of detection of the assay.

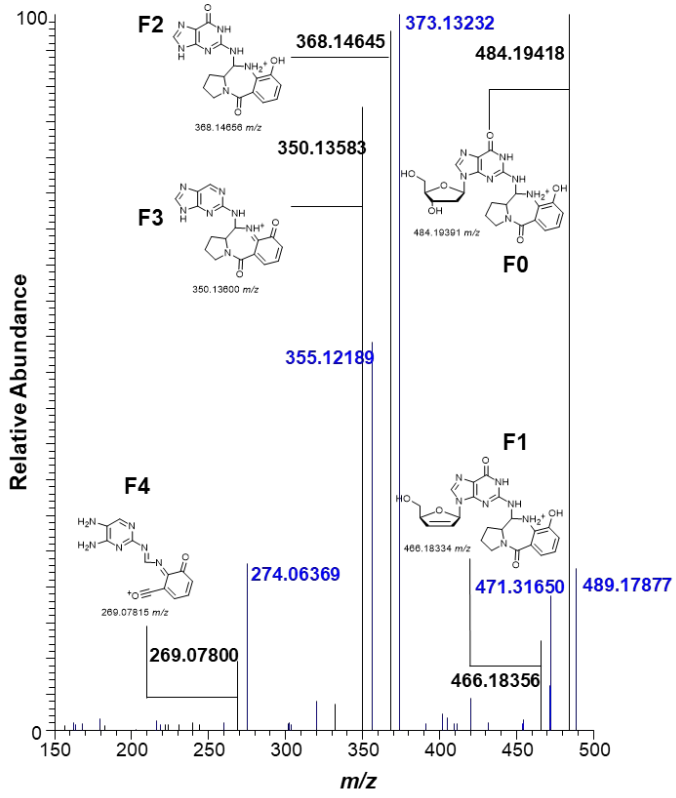

Figure 10. MS^2 Fragmentation pattern of dG-tilimycin adduct (possible structure) from tilimycin exposure to ctDNA (black) overlaid with identical exposure to ^{15}N bacterial DNA (blue). Possible product ions F0-F4 shown.

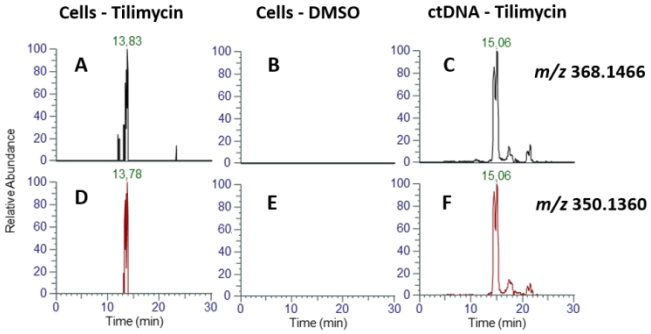

Figure 11. MS^2 EIC of 484.1939→368.1466 *m/z* (neutral loss of deoxyribose) for tilimycin-treated HEK cells (A), DMSO-only HEK cells (B), and tilimycin treated ctDNA (C). MS^2 EIC of 484.1939→350.1360 *m/z* (neutral loss of deoxyribose, H_2O) for tilimycin-treated cells (D), DMSO-only HEK cells (E), and tilimycin-treated ctDNA (F).

DISCUSSION

Tilimycin belongs to a large class of NRPS secondary metabolites called pyrrolobenzodiazepines (PBD) that contain a tricyclic ring system formed by condensation of anthranilic acid and L-proline derivatives.[59] PBDs are largely produced by the *Streptomyces* genus of bacteria and their exceptional cytotoxicity[52] has been exploited to design synthetic PBD dimers as investigational chemotherapeutic agents.[53] Targeted delivery of PBD dimers to tumor cells through antibody-drug conjugate techniques has been investigated in multiple Phase I-III clinical trials.[60–62] Thus, the presence of an endogenously produced PBD within the human microbiota is concerning.[24]

The biosynthesis of prototypical PBDs including anthramycin[59], tomaymycin[63], and sibiromycin[64,65] have been elucidated by functional assignment of the corresponding biosynthetic gene clusters through homology analysis, gene inactivation, and chemical complementation studies. The PBD core is assembled by a bimodular NRPS comprised of a loading module with an adenylation and thiolation domain, either as a single protein or separate stand-alone proteins, and an extension module with a C-A-T-Re architecture. Müller and co-workers recently reported the first attempt to biochemically reconstitute a complete PBD NRPS system using LC-MS to directly detect phosphopantetheine tethered substrates including anthranilic acid and proline derivatives. A dipeptide intermediate attached to the thiolation domain of the extension module was also observed.[63] However, only trace quantities of PBD were produced, which the authors speculated may be due to insufficient channeling between the recombinant NRPS proteins under the *in vitro* assay conditions.[63] We successfully reconstituted the complete tilivalline NRPS employing recombinant NspA, ThdA, and NspB proteins and were able to dissect the activities

of each module using continuous coupled assays that measured production of pyrophosphate or NADPH consumption.

We first interrogated the activity of the loading module, which was greatly facilitated by the unique organization of the tilimycin NRPS system wherein the adenylation and thiolation domains, NpsA and ThdA, are stand-alone proteins, enabling use of stoichiometric quantities of ThdA to promote turnover. Typically, adenylation domain activity is evaluated using a non-physiologically relevant pyrophosphate exchange assay that only measures the first half-reaction in the reverse direction through incorporation of pyrosphosphate into ATP. Instead, we evaluated the loading of ThdA by NpsA by quantifying formation of the pyrophosphate byproduct using a coupled enzyme system consisting of pyrophosphatase and purine nucleoside phosphorylase.[38,40] NpsA catalyzed the efficient loading of ThdA with 3-hydroxyanthranilic acid yielding a k_{cat} of 0.89 s^{-1} and K_M values of 63, 15 and 3.4 μM for 3-hydroxyanthranilic acid, ATP and *holo*-ThdA, respectively. The K_M for *holo*-ThdA is commensurate with other values reported for thiolation domains with their cognate adenylation domains; however, the apparent K_M of ATP and 3-hydroxyanthranilic acid are an order of magnitude lower and higher than related substrates with aryl acid adenylation domains, respectively.[36,41,66] Apparent K_M values determined for these NRPS adenylation enzymes are strongly affected by the assay utilized (hydroxamate-MesG versus the classical pyrophosphate exchange) as well as substrate concentrations, which could explain the observed discrepancies.

We also observed ThdA possessed strong substrate inhibition with a K_i = 15 ± 2 μM. The three dimensional structure of our NpsA:ThdA fusion construct shows the interface between the ThdA loop 1 and the A_{sub} domain of NpsA are composed of many electrostatic and non-specific hydrophobic interactions. These interactions are also conserved in the homologous natural

didomain of the *Xenorhabdus* species.[67] These observations support the hypothesis that the interface observed in the NpsA-ThdA crystal structure is physiologically relevant. This interaction also explains the observed inhibition at high concentrations of ThdA; the substrate binding pocket is occluded by ThdA and A_{sub} when ThdA is bound to NpsA in the thiolation conformation. There may be an equilibrium between adenylation and thiolation conformations that shift in favor of thiolation in the presence of *holo*-ThdA.

Interrogation of NpsB activity proved much more challenging and initial attempts using our coupled assay systems for pyrophosphate or NADPH consumption failed to show any turnover. However, catalytic turnover could be achieved employing stoichiometric concentrations of pre-loaded ThdA as the substrate for NpsB in the presence of the other co-substrates L-proline and NADPH. The time-dependent formation of tilivalline was confirmed by LC-MS analysis employing an authentic synthetic standard. We were able to demonstrate for the first time the efficient production of a PBD *in vitro* with an overall k_{obs} of 0.013 s^{-1} using this product formation assay (**Figure S16**). The inability of NpsB to turnover L-proline in the presence of ATP and NADPH suggests the reductase domain possesses high specificity for the native L-*N*-(3-hydroxyanthraniloyl)prolyl-S~T_{NpsB} intermediate over L-prolyl-S~T_{NpsB}, which stands in stark contrast to other reported Re domains that more rapidly reduce the amino thioester monomers over the corresponding dipeptide thioesters.[68] The close correspondence between the k_{obs} determined in the product formation and the k_{cat} of 0.05 s^{-1} independently determined using a NADPH consumption assay confirm reduction is tightly coupled to dipeptide formation. While the overall k_{cat} is low, it represents a composite of the microscopic rate constants for L-proline adenylation and thioesterification onto the thiolation domain of NpsB, condensation of the resulting L-prolyl-S~T_{NpsB} with the upstream 3-hydroxyanthraniloyl-S~ThdA, and thioester

reduction of the L-*N*-(3-hydroxyanthraniloyl)prolyl-S~T_{NpsB} intermediate to a dipeptide aldehyde species that spontaneously cyclizes to tilimycin as a diastereomeric mixtures of cyclic aminals. We hypothesize the rate-limiting step is likely reductive release since previous studies with Re domains[68,69] show low turnover numbers (apparent k_{cat}'s ranging from 0.03 to 0.003 sec^{-1}). By contrast, the reaction rates of isolated adenylation and condensation domains are typically two-to-three orders of magnitudes greater than our observed k_{cat}.[39,50,68,70,71]

The major metabolite isolated from *K. oxytoca* in cell culture as well as the gut microbiome is not tilimycin, but rather tilivalline due to non-enzymatic and irreversible reaction of tilimycin with indole by electrophilic aromatic substitution.[24,29,33] The reaction proceeds through an iminium species produced by dehydration of tilimycin. The initial report by Zechner and co-workers identified tilivalline as the major metabolite produced by *K. oxytoca*; however, subsequent studies have shown tilimycin is also formed *in vitro* and *in vivo*.[29,33] Tilimycin is an order of magnitude more cytotoxic than tilivalline and is also a genotoxic DNA-damaging agent, whereas tilivalline inhibits microtubule formation.[33] Consequently, tilimycin likely plays a more significant role in AAHC and may additionally lead to cellular transformation upon long-term exposure.[33]

Interestingly, the relationship between the dipeptides tilimycin and tilivalline, which are produced by enzymatic and non-enzymatic processes and mediate different cellular effects, bears similarity to other NRPS systems. Fischbach et al. has shown that NRPS biosynthetic gene clusters harboring terminal reductase domains that afford dipeptide aldehydes are ubiquitous in the gut microbiota.[72] Dipeptide aldehydes produced in the gut can potentially modulate host-microbe interactions through inhibition of cysteine proteases.[72] Cyclization of typical dipeptide aldehydes lacking an anthranilate moiety occurs slowly over several hours in the gut yielding

dihydropyrazinone and pyrazinone metabolites, which are predicted to have important physiological roles in mediating microbe-microbe interactions.[68,73]

In parallel to our characterization of NpsA we synthesized the bisubstrate inhibitors 3-hydroxyanthraniloyl-AMS **5**, 3-hydroxybenzoyl-AMS **8** and anthraniloyl-AMS **9**. Biophysical characterization by isothermal titration calorimetry revealed the 3-hydroxyl of the aryl ring is more important than the 2-amino substituent since removal of the 3-hydroxyl group in **8** led to a greater than 20-fold loss of affinity and concordant 4 kcal/mol decrease in binding enthalpy. The ITC result is consistent with the removal of the two hydrogen bonds (Asn207/Ser271) that could contribute ~2 kcal/mol each to binding enthalpy as seen in the co-crystal structures. By contrast, deletion of the 2-amino group in **9** led to no reduction in binding enthalpy and a modest 4-fold reduction in affinity that can be attributed to an entropic penalty from removal of the possible prearrangement via intramolecular hydrogen bonding between the 2-amino and the *N*-acyl sulfamide. The trend in binding affinities for 3-hydroxybenzoyl ligand **8** (K_D = 112 nM) and anthraniloyl ligand **9** (K_D = 485 nM) is counterintuitively opposite the trend in K_M values for the respective substrates 3-hydroxybenzoic acid (K_M = 4,000 μM) and anthranilic acid (K_M = 854 nM) with NpsA. These results indicate the 3-hydroxy is more critical for binding, whereas the 2-amino group is important for catalytic efficiency.

The design of inhibitors of specific enzymes in gut microbial pathways mechanistically linked to human diseases represents a novel strategy to develop a new class of pharmacological agents.[74–76] The tilimycin pathway has been genetically validated for causing AAHC.[24] Moreover, tilimycin and many PBDs are potent genotoxins,[33] thus small-molecule inhibitors of tilimycin biosynthesis could have therapeutic utility for not only treating AAHC, but also to prevent transformation of colorectal cells in the 2–10% of people colonized with *K. oxytoca*.

Attempts to 'drug the microbiome' are still in the early stages of conception; however, non-antibiotic approaches may have utility, especially in light of the rise of antimicrobial resistance and the revolution of precision medicine.[77,78] As a prelude to future studies for treating AAHC, we evaluated our bisubstrate inhibitors for inhibition of tilimycin in *K. oxytoca* cell cultures. We initially examined our most potent enzyme inhibitor 3-hydroxyanthraniloyl-AMS **5** against *K. oxytoca* and were dismayed to observe no inhibition of tilimycin production. We speculated the lack of activity may be due to oxidative degradation of the *ortho*-aminophenol moiety of 3-hydroxyanthraniloyl-AMS **5** under the aerobic culture conditions.[79] Indeed, we observed rapid degradation of **5** under the culture conditions, so we examined 3-hydroxybenzoyl-AMS **8** and anthraniloyl-AMS **9** that lack the sensitive *ortho*-aminophenol moiety. Consistent with its improved biochemical potency, 3-hydroxybenzoyl-AMS **8** was found to possess superior activity inhibiting 50% tilimycin production at 29 μM, but no observable growth inhibition of *K. oxytoca* at 300 μM, the highest concentration evaluated. Previous studies of related adenylation inhibitors have shown they possess poor bioavailability and thus are expected to accumulate to high levels in the gastrointestinal tract.[45] Consequently, inhibitors such as **8** may have ideal characteristics for selective inhibition of tilimycin inhibition while sparing both the host and the microbiome.

PBDs share a common mechanism of action through the covalent binding to guanosine in double-stranded DNA, which was established by a series of seminal studies in the 1970s.[57,80] A single X-ray co-crystal structure of anthramycin bound to the synthetic oligonucleotide 5′-CCAACGTTGG-3′ confirmed anthramycin binds in the minor groove and alkylates N-2 of the guanine nucleobase.[81] However, limited binding is available for most PBDs and DNA interaction is inferred using molecular modeling and thermal stabilization assays measuring unfolding of double-strand DNA with short synthetic oligonucleotides.[82–86] A few recent studies have

quantified overall DNA binding using mass spectrometry, but detection of defined DNA adducts *in vivo* has never been reported for any PBD.[87,88] To this end, we sought to identify for the first time, PBD-like DNA adducts caused by tilimycin exposure to eukaryotic cells. The major metabolite observed in calf thymus DNA and HEK cell exposure was the hypothesized dG-tilimycin adduct with a parent mass of 484.1939 *m/z*. This molecular weight supports the previous reports of the N-2 regioselective alkylation of guanine. The N-7 of guanine is the most nucleophilic nitrogen on the nucleobase, however, when alkylation of the N-7 occurs, like in the case of nitrogen mustards, the anomeric linkage is weakened and the 2′-deoxyribose is rapidly cleaved. In the case of tilimycin, the parent mass of this N-7 metabolite would be 368.1467 *m/z* (-ribose), which was not observed. MS^3 fragmentation of the dG-tilimycin adduct reveals a unique fragment with a mass of 269.0789 *m/z*. We hypothesized that this fragment was a result of loss of pyrrolidine from tilimycin which maintained the aminal linkage to guanine. When calf thymus DNA was exposed to high levels of tilimycin we were also able to detect a novel dA-tilimycin adduct. This adduct was not detectable in the exposure of tilimycin to HEK cells, which may indicate a higher sensitivity requirement to monitor the low abundance of the metabolite.

CONCLUSION

Although pyrrolobenzodiazepines were discovered nearly sixty years ago and have been extensively studied, fundamental questions remained concerning their biosynthesis and mechanism of action. In this study we sought to more fully characterize the NRPS biosynthetic machinery and mechanism of action of the microbiota-derived metabolite, tilimycin. We provided the first kinetic characterization of a bimodular NRPS responsible for PBD biosynthesis. First, we established that NspA efficiently loads ThdA with a preference for

anthranilate and demonstrated the 2-amino group is more critical than the 3-hydroxyl group for catalytic efficiency. Unexpectedly, we showed ThdA exhibits strong substrate inhibition by occluding the substrate binding pocket of NpsA. We next studied the extension module NpsB and showed it orchestrates the biosynthesis of tilimycin in a tightly controlled manner with reductive release only occurring on the dipeptide chain intermediate to afford a dipeptidyl aldehyde that spontaneously cyclizes to tilimycin. The bisubstrate AMS and AVS inhibitors proved crucial for the structural characterization of NpsA and ThdA and allowed us to observe both the adenylation and thioester conformations of NpsA. As a potential therapeutic strategy for treating antibiotic associated hemorrhagic colitis, we showed 3-hydroxybenzoyl-AMS **8** could completely block biosynthesis of tilimycin in *K. oxytoca* providing a nonmicrobiocidal approach to drugging the microbiome. Finally, in order to conclusively characterize the mechanism of action of tilimycin, we detected the pyrrolobenzodiazepine-like N-2 deoxyguanine adduct when HEK cells were exposed to tilimycin and detected a novel deoxyadenosine DNA adduct when exposed calf thymus DNA to tilimycin. To the best of our knowledge, this is the first structural characterization of a PBD-DNA adduct formed in cells.

Methods

Cloning: The *K. oxytoca* gene encoding for NpsA (NpsA; WP_004103551.1) was commercially synthesized (GENEWIZ, South Plainfield, NJ) containing NdeI (5′) and XhoI (3′) restriction sites appended to the ends of the gene. A single silent mutation was designed at the codon for Ala5 to eliminate a natural NdeI site contained within the gene. The gene was subcloned using NdeI/XhoI) into a pET15b vector containing an N-terminal 5xHis-tag and TEV protease recognition site (pET15b-TEV-NpsA; Genewiz; South Plainfield, NJ, USA). *K. oxytoca* strain MIT-5243 was obtained from BEI Resources (Manassas, VA) and grown in small cultures for the generation of genomic DNA. The genes encoding ThdA and NpsB were PCR amplified from genomic DNA and cloned into the pET15b-TEV plasmid using NdeI and XhoI restriction sites.

Protein expression and purification. Wild-type (wt)-*NpsA*. The ampicillin-resistant pET15b-wt-NpsA plasmid was transformed into BL21(DE3) cells for expression. A single colony from the transformed cells was used to inoculate a 3 mL starter culture of LB containing ampicillin (100 μg/mL). The starter culture was grown overnight at 37 °C with shaking at 250 rpm. The following day, the 3 mL culture was used to inoculate 1 L of terrific broth (24 g/L yeast extract, 20 g/L tryptone, 4 mL/L glycerol, 0.017 M KH_2PO_4, 0.072 M K_2HPO_4) containing ampicillin (100 μg/mL). The culture was shaken at 250 rpm and 37 °C until the OD_{595} reached 0.8, then the temperature was lowered to 16 °C and the culture induced with IPTG (750 μM) and incubated overnight at 16 °C with shaking at 250 rpm.

Cells were harvested by centrifugation (5,000×g, 20 min, 4 °C), resuspended in lysis buffer (50 mM HEPES, 150 mM NaCl, 20 mM imidazole, 0.2 mM TCEP, pH 6.8) and lysed by French press. The lysed cells were centrifuged (35,000×g, 40 min, 4 °C) and the supernatant was loaded onto Ni-NTA resin (2 mL, Takara; Mountain View, CA. USA). The resin was washed with lysis

buffer (10 mL). wt-NpsA was eluted with elution buffer (50 mM HEPES, 150 mM NaCl, 300 mM imidazole, 0.2 mM TCEP, pH 6.8) and subsequently loaded onto a HiLoad 16/600 Superdex 75 pg gel-filtration column (GE Healthcare) using SEC buffer (50 mM HEPES, 150 mM NaCl, 0.2 mM TCEP, 10% glycerol, pH 6.8). The fractions containing NpsA were pooled, exchanged into storage buffer (25 mM HEPES, 75 mM NaCl, 0.2 mM TCEP, 10% glycerol, pH 6.8) and concentrated using a 10 kDa centrifugation. The resulting protein stock was stored at -80 °C and thawed prior to use.

ThdA. Expression was the same as wt-NpsA with the following exceptions: After IMAC chromatography the partially purified protein was incubated with TEV protease (8% w/w) and dialyzed in 50 mM HEPES, 250 mM NaCl, 0.2 mM TCEP, pH 8.0 buffer for 16 h at 4 °C. Further incubation of ThdA with the promiscuous phosphopantethineyl transferase Sfp (10 nM), 12.5 mM $MgCl_2$ and 1 mM CoA for 60 minutes at 24 °C ensured full conversion of *apo*-ThdA to *holo*-ThdA.[49,89] The storage buffer was (20 mM HEPES, 40 mM NaCl, 0.2 mM TCEP, pH 7). *holo*-ThdA was concentrated using a 10 kDa centrifugation filter and fractionated into 20 µL aliquots frozen at -80 °C until used. The total protein yield was determined by nanodrop to be 26.5 mg/L of culture.

NpsB. The ampicillin-resistant pET15b-NpsB plasmid was transformed into BL21(DE3) cells for expression. A single colony from the transformed cells were used to inoculate a 3 mL starter culture of LB containing ampicillin (100 µg/mL). The starter culture was grown overnight at 37 °C with shaking at 250 rpm. The following day, the 3 mL culture was used to inoculate 1 L of terrific broth (24 g/L yeast extract, 20 g/L tryptone, 4 mL/L glycerol, 0.017 M KH_2PO_4, 0.072 M K_2HPO_4) containing ampicillin (100 µg/mL). The culture was shaken at 250 rpm and 37 °C until

the OD_{595} reached 0.6, then the temperature was lowered to 16 °C and the culture induced with IPTG (250 μM) and incubated overnight at 16 °C with shaking at 250 rpm.

Cells were harvested by centrifugation (5,000×g, 20 min, 4 °C), resuspended in lysis buffer (50 mM HEPES, 250 mM NaCl, 20 mM imidazole, 0.2 mM TCEP, 10% glycerol, pH 6.8) and lysed by French press. The lysed cells were centrifuged (35,000×g, 40 min, 4 °C) and the supernatant was loaded onto Ni-NTA resin (2 mL, Takara; Mountain View, CA. USA). The resin was washed with lysis buffer (10 mL). NpsB was eluted with elution buffer (50 mM HEPES, 250 mM NaCl, 300 mM imidazole, 0.2 mM TCEP, 10% glycerol, pH 6.8) and subsequently loaded onto a HiLoad 16/600 Superdex 200 pg gel-filtration column (GE Healthcare) using SEC buffer buffer (50 mM HEPES, 250 mM NaCl, 0.2 mM TCEP, 10% glycerol, pH 6.8). The fractions containing NpsB were pooled, exchanged into storage buffer (50 mM HEPES, 150 mM NaCl, 0.2 mM TCEP, 10% glycerol, pH 6.8) and concentrated using a 10 kDa centrifugation filter. The resulting protein stock was stored at -80 °C and thawed prior to use. The total protein yield was 2.7 mg/L of culture.

NpsA Assay. Reactions were performed under initial velocity conditions using wt-NpsA (20–200 nM), 0.1 U purine nucleoside phosphorylase (Sigma N8264-100UN), 0.04 U inorganic phosphatase (Sigma I1643-100UN), and 100 μM MesG (Berry & Associates), with varying concentrations of ATP, aryl acid, and ThdA in assay buffer (50 mM Tris, 150 mM NaCl, 10 mM $MgCl_2$, pH 8) in a total volume of 100 μL. The reaction was initiated by addition of wt-NpsA. Reactions were run in triplicate in 96 half-area UV transparent plates (Corning 3679) and cleavage of MesG was continuously monitored at A_{360} every 10 sec on a Molecular Devices Spectra Max M5e over 5 min.

Determination of Kinetic Parameters and Substrate Specificity of NpsA. Steady-state kinetic parameters of aryl acids, ATP and *holo*-ThdA were determined using the wt-NpsA assay described above by varying one substrate concentration while maintaining the other two substrates at fixed saturating levels. The enzyme and substrate concentrations for kinetic characterization were: aryl acid (7.8–1000 μM) with ATP (5 mM) and ThdA (20 μM) held constant employing 200 nM wt-NpsA; ATP (7.8–1000 μM) with aryl acid (500 μM) and ThdA (20 μM) held constant employing 20 nM wt-NpsA; and ThdA (0.31–80 μM) with aryl acid (500 μM) and ATP (5 mM) held constant employing 20 nM wt-NpsA. The normalized initial velocities from triplicate experiments were then plotted against the varied substrate concentration to generate a saturation curve, which was fit by nonlinear regression analysis to the Michaelis-Menten equation (eq 1) or the substrate inhibition model (eq 2) using GraphPad Prism 6.0.

$$v_0 = \frac{v_{max}[S]}{K_M + [S]} \quad (1)$$

$$v_0 = v_{max}\frac{[S]}{K_M + [S]\left(1 + \frac{[S]}{K_i}\right)} \quad (2)$$

Measurement of Inhibition Constants. The determination of the apparent inhibition constants (appK_i) for adenylation inhibitors **5**, **8** and **9** was performed using the NpsA assay described above and performed in triplicate. All inhibitors were tested from 11–1000 nM at a constant 1% DMSO concentration with 20 nM wt-NpsA in the presence of saturating concentrations of 3-hydroxyanthranilic acid (500 μM), ATP (5 mM) and ThdA (20 uM). The inhibitors displayed tight-binding inhibition ($K_i^{app} < 200 \cdot [E]$), thus the fractional activity (v_i/v_0), where v_i is the reaction velocity at a given [I] and v_0 is the reaction velocity of the DMSO control, were fit by nonlinear regression analysis using GraphPad Prism 6.0 to the Morrison equation (eq 3),[90] constraining [E] to 20 nM to obtain the appK_i values, which were converted to K_i values using

the Cheng-Prushoff equation (eq 4) for a competitive inhibitor, where [*S*] and K_M correspond to the concentration and Michaelis constant of 3-hydroxyanthranilate.

$$v_i/v_0 = 1 - \frac{([E]_T + [I]_T + K_i^{app}) - \sqrt{([E]_T + [I]_T + K_i^{app})^2 - 4[E]_T[I]_T}}{2[E]_T} \quad (3)$$

$$K_i^{app} = K_i(1 + \frac{[S]}{K_M}) \quad (4)$$

Determination of Kinetic Parameters of NpsB. Steady-state kinetic parameters of L-proline, ATP and NADPH were determined by monitoring NADPH consumption (ΔA_{340}) with or without the presence of NpsA (20 nM), ThdA (20 μM), and 3-hydroxyanthranilic acid (500 μM) in assay buffer (50 mM Tris, 150 mM NaCl, 10 mM $MgCl_2$, pH 8). The enzyme and substrate concentrations for kinetic characterization were: L-proline (0.078–10 mM) with ATP (5 mM) held constant employing 250 nM NpsB; ATP (7.8–500 μM) with L-proline (5 mM) held constant employing 250 nM NpsB; and NADPH (7.8–250 μM) with L-proline (5 mM) and ATP (5 mM) held constant employing 250 nM NpsB. The initial velocities from triplicate experiments were then plotted against the varied substrate concentration to generate a saturation curve, which was fit by nonlinear regression analysis to the Michaelis-Menten equation (eq 1).

Isothermal Titration Calorimetry. ITC experiments were performed on an AutoITC$_{200}$ (Malvern Instruments). The experiments were performed at 25 °C in assay buffer (50 mM HEPES, 150 mM NaCl, 5 mM $MgCl_2$ pH 6.8). Buffer exchange into assay buffer was performed on wt-NpsA prior to experiments using centrifugation filtration (Amicon 10 kDa filter) and the final filtrate was used to prepare a solution of the inhibitors from a 50 mM stock in DMSO. The percentage DMSO in the final inhibitor solution was matched in the wt-NpsA protein solution. The 200 μL sample cell was filled with wt-NpsA (30 μM, concentration determined using the calculated extinction coefficient Protparam tool) and the 40 μL injection syringe was filled with inhibitor

(300 μM). Titrations were carried out with a stirring speed of 750 rpm and a 200 s interval between 2 μL injections. The first injection for each sample was excluded from data fitting. The experimental data was fitted to a titration curve using the Origin™ software package (version 7.0) to determine K_A, n, and ΔH. The thermodynamic parameters (ΔG and $T\Delta S$) were calculated using equation 5:

$$\Delta G = -RTln(K_A) = \Delta H - T\Delta S \quad (5)$$

where ΔG, ΔH, and ΔS are the changes in free energy, enthalpy, and entropy of binding, respectively; R = 1.98 cal·mol^{-1}K^{-1}; T is the absolute temperature (298 K). The affinity of the ligands for the protein is given as the dissociation constant ($K_D = 1/K_A$). ITC experiments were run in triplicate and analyzed independently, and the thermodynamic values were averaged.

Inhibition of Tilivalline Biosynthesis in K. oxytoca. Production of tilivalline by *K. oxytoca* (BEI Resources, MIT 10-5243) was performed in duplicate in 14 mL snap-cap tubes containing 3-mL cultures in CASO medium (17 g/L casein peptone, 2.5 g/L K_2HPO_4, 2.5 g/L, D(+)-glucose, 5 g/L NaCl, 3 g/L soy peptone). Cultures were incubated at 37 °C at 250 rpm. Prior to every experiment, *K. oxytoca* was streaked out on an LB-ampicillin agar plate and one colony was chosen for the subsequent experiments. Cultures were inoculated with an overnight CASO culture from a single colony to a starting OD_{600} = 0.01 with varying concentrations of **5**, **8** and **9** or 0.6% DMSO as a negative control. Aliquots (20 μL) of the cultures were taken at 8 and 24-hour timepoints. The aliquots were diluted with 80 μL acetonitrile, vortexed for 20 sec and stored at -20 °C for 2 h to ensure full precipitation. The solutions were centrifuged at 15,000×g for 5 min and 50 μL of the supernatant was transferred to a conical vial containing 50 nM benzyl-tilivalline as an internal standard. The samples were then subjected to LC-MS/MS analysis.

Tilivalline Quantitation. Samples were analyzed by LC-MS/MS (Shimadzu UFLC XR-AB SCIEX QTRAP 5500). Reverse phase LC was performed on a Kinetix C18 column (50 mm × 2.1 mm, 2.6 μm particle size; Phenomenex, Torrance, CA). Mobile phase A was 0.1% aqueous formic acid while mobile phase B was 0.1% formic acid in acetonitrile. Initial conditions were 5% B from 0 to 0.5 min, after which the %B was increased to 95% from 0.5 to 3 min. The column was washed in 95% B for 2 min, returned to 5% over 0.2 min, and allowed to re-equilibrate for 2.8 min in 5% B to provide a total run time of 8 min. The flow rate was 0.5 mL/min and the column oven was maintained at 40 °C. The injection volume was 10 μL. Tilivalline was monitored by MS in positive ionization mode by multiple reaction monitoring (MRM). To determine the optimum mass spectrometry settings, an authentic tilivalline standard was infused at a concentration of 1 μM (1:1 water/acetonitrile containing 0.1% formic acid) onto the MS by a syringe pump at a flow of 10 μL/min. The following transitions were utilized: 334.4→199.1 [tilivalline (analyte)] 424→199.1 [benzyl-tilivalline (internal standard)]. Analyte and internal standard peak areas were calculated (MultiQuant, version 2.0.2, AB SCIEX). Analyte peak areas were normalized to internal standard peak areas, and the analyte concentrations were determined with an appropriate standard curve.

Cloning, expression, and purification of NpsA, NpsA-N and NpsA-ThdA fusion protein for X-ray crystallography. Wt-NpsA proved refractory to initial crystallization attempts with an in-house sparse matrix screen. To enhance the probability of successful crystal nucleation and growth, a surface entropy reduction (SER) mutation, EEQ→AAA, was identified with the SERp server and introduced at positions 312-314 via QuikChange mutagenesis. All subsequent constructs generated for crystallographic analysis contain this EEQ→SER mutation. A construct encoding NpsA with the C-terminal subdomain, A_{sub} (Asn405-Val506), removed was also

cloned into pET15b-TEV and designated pET15b-TEV-NpsA-N. The artificial di-domain fusion construct encoding for NpsA-ThdA was cloned by inserting the ThdA gene with a six bp 5′ linker encoding for the insertion of an Ala-Ser dipeptide at the 3′ end of NpsA to generate pET15b-TEV-NpsA-ThdA (Figure **S8–S12**).

NpsA, NpsA-ThdA, and NpsA-N for crystallization studies were produced in *E. coli* BL21(DE3) cells. 1 L of LB media (100 μg/mL ampicillin) was inoculated with 1 mL of an LB overnight culture (100 μg/mL ampicillin, 37 °C, 250 rpm). Cultures were grown to an OD_{600} of approximately 0.6 (37 °C, 250 rpm) then incubated at 4 °C (30 min, 250 rpm) after which IPTG (500 μM) was added followed by incubation at 16 °C (20 h, 250 rpm). Cells were harvested via centrifugation (5000×g, 35 min, 4 °C) and flash frozen in liquid nitrogen. Subsequent purification steps were carried out at 4 °C.

Cell pellets were resuspended in lysis buffer (NpsA, NpsA-N; 50 mM HEPES pH 8.0, 150 mM NaCl, 20 mM imidazole, 0.2 mM TCEP; 10 mL/g) or lysis buffer with 10% v/v glycerol (NpsA-ThdA; 20 mL/g). Cells were lysed via mechanical disruption (Branson sonifier) and the resulting lysate was clarified via ultracentrifugation (40,000×g, 40 min, 4 °C), filtered (0.45 μm) and passaged over a Ni-loaded HisTrap column followed by a 3 column volume (CV) washout with lysis buffer. The column was then washed with 5 CVs of 10% v/v elution buffer (NpsA, NpsA-N; 50 mM HEPES pH 8.0, 150 mM NaCl, 300 mM imidazole, 0.2 mM TCEP) or elution buffer with 10% v/v glycerol (NpsA-ThdA) followed by a linear gradient of 10→100% v/v elution buffer over 5 CVs. For NpsA-N, protein-laden fractions were pooled, TEV protease was added (1:100 w/w, TEV:NpsA/NpsA-N), and then fraction pools were dialyzed against lysis

buffer for approximately 16 h. TEV protease and uncleaved NpsA-N were removed by a second passage over the Ni-loaded HisTrap column following the initial day 1 procedure.

NpsA-ThdA was subjected to simultaneous TEV cleavage and phosphopantetheinylation. Following day 1 Ni-IMAC, NpsA-ThdA containing fractions were pooled and combined with TEV protease (1:100 w/w, TEV:NpsA-ThdA), promiscuous phosphopantetheinyl transferase Sfp (400 nM), $MgCl_2$ (1 mM), and coenzyme A (1 mM; ~5 equivalents NpsA-ThdA). The reaction mixture was rocked gently at 23°C for 3 h and then dialyzed against lysis buffer (4 h, 4°C). TEV protease, Sfp, and uncleaved NpsA-ThdA were removed by a second passage over the Ni-loaded HisTrap column following the initial day 1 procedure. Following the final IMAC purification step fraction pools were concentrated (Amicon® Ultra Filter; NpsA/NpsA-N: 30 kDa MWCO, NpsA-ThdA: 50 kDa MWCO) and further purified via gel filtration (Superdex200, 16/60; NpsA, NpsA-N: 50 mM HEPES pH 8.0, 150 mM NaCl, 0.2 mM TCEP; NpsA-ThdA: 50 mM HEPES pH 8.0, 150 mM NaCl, 0.2 mM TCEP, 10% v/v glycerol; **Figure S14**. Following gel filtration samples were exchanged to a crystallization buffer (NpsA: 10 mM HEPES pH 8.0, 25 mM NaCl, 0.4 mM TCEP; NpsA-ThdA: 10 mM HEPES pH 8.0, 25 mM NaCl, 0.4 mM TCEP, 2.5 mM $MgCl_2$, 5% v/v glycerol) via serial concentration and dilution or concentrated directly in gel filtration buffer (NpsA-N). Final protein concentrations (NpsA-N: 15.0 mg/mL, NpsA: 7.0 mg/mL, *holo*-NpsA-ThdA: 19.0 mg/mL) were determined using extinction coefficients at 280 nm (NpsA-N: 31860 $M^{-1}cm^{-1}$, NpsA: 38850 $M^{-1}cm^{-1}$, *holo*-NpsA-ThdA: 44350 $M^{-1}cm^{-1}$). NpsA-N and NpsA-ThdA samples protein samples were flash frozen as pellets in liquid nitrogen and stored at -80°C. NpsA protein samples were stored at 4°C for approximately 2 days prior to crystallization plate setup.

Crystallization of NpsA variants. *NpsA-N*. Unliganded NpsA-N crystals were grown with hanging drop vapor diffusion at 20 °C. Thawed NpsA-N stock solution (15 mg/mL, 1 μL) was mixed with well solution (100 mM HEPES pH 7.5, 150 mM KBr, 30% w/v PEG3350, 1 μL) and the resultant drop was incubated over 500 μL of well solution in a 24-well linbro style plate. Unliganded NpsA-N crystals were cryoprotected by soaking in well solution supplemented with 15% v/v glycerol for approximately 15-30 seconds prior to vitrification in liquid nitrogen. 3-hydroxyanthraniloyl-AMS **5**, 3-hydroxybenzoyl-AMS **8** and anthraniloyl-AMS **9** ligands were introduced into unliganded NpsA-N crystals following the same general cryoprotection/soaking procedure. Three separate solutions containing increasing PEG3350 concentration (34, 41, 48% w/v), 100 mM HEPES pH 7.5, and 150 mM KBr, were supplemented with 2 mM **5**/**8**/**9**. Ligand stock solutions (50 mM) were prepared with either gel filtration buffer (**5**/**8**) or DMSO (**9**). The NpsA-N crystals were harvested and soaked for approximately 1 h in each PEG3350 solution in order of increasing PEG concentration at 23 °C. During each soaking step drops were sealed in a 72 well microbatch plate with paraffin oil. Crystals were vitrified directly in liquid nitrogen after the final soak.

NpsA. Crystals of full length NpsA were grown in the presence of **5** using the microbatch under paraffin oil technique at 23 °C. NpsA stock solution was concentrated (10 kDa MWCO Amicon® filter) and combined with a **5** stock solution (30 mM in NpsA crystallization buffer) so that the composition of the final solution was 16 mg/mL NpsA, 5 mM **5** in NpsA crystallization buffer. The NpsA/**5** solution (2 μL) was combined with well solution (400 mM imidazole pH 6.6, 10% w/v PEG HMW, 2.5% w/v 1,3-dimethylimidazolium dimethyl phosphate; PEG HMW is a 1:1:1:1 mixture of PEG8000/10000/12000/20000; 1 μL) and the resultant drop was overlaid with paraffin oil in an untreated, polystyrene 72 well microbatch plate from Hampton Research

(Aliso Viejo, CA, USA). Crystals, which formed concurrently with heavy precipitate, were extracted from the drops and soaked for approximately 5 min in a solution of well solution supplemented with 25% v/v pentaerythritol propoxylate (5/4 PO/OH; PEP426) prior to vitrification in liquid nitrogen.

NpsA-ThdA. *Holo*-NpsA-ThdA was crystallized in the presence of a 3-hydroxybenzoyl-AVS **13** inhibitor using the microbatch under paraffin oil technique at 14 °C. A stock solution of **13** (160 mM, DMSO) was added directly to a thawed solution of *holo*-NpsA-ThdA (19 mg/mL, 300 μM) in approximately 4-fold excess (1.2 mM). The resultant NpsA-ThdA/**13** solution was incubated on ice for approximately 30 min and then filtered (0.2 μm) prior to crystallization plate setup. The protein/ligand solution (1.2 μL) was mixed with well solution (0.2 M sodium formate, 20% w/v PEG3350; 1 μL) and overlaid with paraffin oil. Crystals began to form approximately 1-2 h after plate setup. (+/-)-2-Methyl-2,4-pentanediol (neat, ~1 μL) was added directly to the drop and after approximately 5 min crystals were harvested and vitrified in liquid nitrogen.

X-ray diffraction data collection, structure solution, and refinement. Diffraction data were collected from single crystals on either APS beamline 23-IDD (unliganded NpsA-N, NpsA-N/**5**, NpsA-N/**8**, NpsA/**9**), SSRL beamline 12-2 (NpsA-ThdA/**13**), or SSRL beamline 9-2 (NpsA-N/**5**) (**Table S1**). In each case data were indexed and integrated with XDS followed by merging in the appropriate space group with AIMLESS. Optimal processing parameters were generated with the AutoPROC software package.

NpsA-N. Two separate datasets were collected for unliganded NpsA-N crystals, which occurred in distinct monoclinic space groups with unit cell constants that corresponded to one (*C*2) or two ($P2_1$) chains in the asymmetric unit. Each structure was solved via molecular replacement. A protein basic local alignment search tool (BLAST) search of the protein data

bank (PDB) yielded 53 sequences ranging from 22–33% identity. Due to the lack of a clearly distinguished homology model, the program *MRage,* as implemented in the PHENIX suite, was used to identify a viable search model from among the BLAST results and to solve the NpsA-N *C*2 structure. Ultimately, a solution to the *C*2 structure was found using a search model derived from 1AMU[91] (29% identity with NpsA; phenylalanine activating domain of gramicidin synthase 1) processed with *phenix.sculptor* and with the C-terminal subdomain removed. To improve these initial phases the structure was solved and rebuilt with MR-Rosetta and *phenix.autobuild* using the sculpted 1AMU N-terminal domain as a search model. Portions of the model were rebuilt manually with iterative real space refinement in Coot and reciprocal space refinement in *phenix.refine*. Final rounds of refinement employed translation-libration-screw (TLS) parameterization. The $P2_1$ unliganded NpsA-N structure was solved with two chains in the asymmetric unit using *Phaser* and the *C*2 unliganded NpsA-N structure as a search model. NpsA-N crystals soaked with **5**, **8**, and **9** each crystallized in space group $P2_1$ with unit cell constants that were consistent with those of the unliganded NpsA-N $P2_1$ crystal. For both liganded structures a copy of the two chain unit from the unliganded NpsA-N $P2_1$ structure was placed in the unit cell with *Phaser* followed by iterative real space refinement with Coot and reciprocal space refinement with *phenix.refine*. Ligand restraints for **5**, **8**, and **9** were generated with AM1 optimization as implemented in *phenix.elbow*.[92] Final rounds of refinement employed translation-libration-screw (TLS) parameterization.

NpsA. Full-length NpsA was co-crystallized with **5** in space group *I*222 and with one chain in the asymmetric unit. The structure was solved via molecular replacement using *Phaser* and a single chain unliganded NpsA-N ($P2_1$) search model. Difference density (mF_o-DF_c) corresponding to the C-terminal subdomain was observed after an initial round of coordinate and

atomic displacement parameter (ADP) refinement with *phenix.refine*. The C-terminal subdomain, A_{sub}, was built in manually using the C_α-baton building mode in Coot. Following manual placement of A_{sub} and several rounds of iterative real space refinement in Coot and reciprocal space refinement in *phenix.refine* and *phenix.rosetta_refine* the structure was subjected to molecular dynamics flexible fitting (MDFF) with the *ChimeraX* plugin ISOLDE[93]. Map coefficients ($2mF_o$-DF_c) for real space MDFF via ISOLDE were generated with *phenix.maps* by filling in missing F_{obs} reflections and excluding R_{free} flagged reflections. Following MDFF in ISOLDE, ADP values were refined with *phenix.refine*. Final rounds of refinement employed TLS parameterization; the C-terminal subdomain, A_{sub}, was excluded from TLS refinement.

NpsA-ThdA. NpsA-ThdA co-crystallized with the mechanism-based inhibitor **13** in space group *P*1 with four chains in the asymmetric unit. The structure was solved via molecular replacement using *Phaser* and a single chain unliganded NpsA-N ($P2_1$) search model. Difference density (mF_o-DF_c) corresponding to A_{sub} and ThdA (PCP domain) was observed after an initial round of coordinate and atomic displacement parameter (ADP) refinement with *phenix.refine*. A_{sub} and ThdA domains were built in manually to varying degrees among the four chains with iterative rounds of real space and reciprocal space refinement using Coot and *phenix.refine* respectively. Following this initial refinement problematic regions of the model, *i.e.* rotamer and Ramachandran outliers, were relaxed with ISOLDE into a static $2mF_o$-DF_c map generated with *phenix.maps* with R_{free} flagged reflections excluded and missing F_{obs} reflections filled. Ligand restraints were generated with *phenix.elbow* for a single entity comprised of a phosphopantetheine arm covalently tethered to **13**. Tetrahedral bond restraints were applied to the phosphopantetheine/Ser542 phosphodiester bond. Final rounds of refinement included bond

length and angle outlier correction with *phenix.real_space_refine* followed by ADP refinement and TLS parameterization in *phenix.refine*; A_{sub} and ThdA domains were excluded from TLS refinement.

Alamar Blue Cell Viability Assay. Human embryonic kidney cell (HEK293T, ATCC: CRL-3216) cells were cultured in Dulbecco's minimum essential medium (MEM) supplemented with 10% (v/v) fetal bovine serum, 100 U/mL penicillin and 100 μg/mL streptomycin under a 5% CO_2 atmosphere at 37 °C. Cells were seeded into a 96 well plate (Corning 3595) at a density of 10,000 cells/well. After incubation for 24 h, the media was removed from adherent cells and replaced with FBS free MEM containing tilimycin yielding a final concentration of 0.125, 0.25, 0.5, 1, 2, 4, 8, 16, 32, 64, 128 μM tilimcyin or DMSO (0.2%) and subsequently allowed to incubate for an additional 24 h. All experiments were performed in triplicate for each concentration. Following the 24 h incubation, 10 μL of alamar blue cell viability reagent (Invitrogen A50100) was added. The plate was further incubated for 4 h in the dark at 37 °C after which fluorescence was measured at Ex_{560}/Em_{590} 560:590 on a Molecular Devices Spectra Max M5e plate reader. Cell viability was calculated by normalizing fluorescence signal to the DMSO treated control (**Figure S13**).

Reagents for DNA Adductomics. Methanol (LC-MS grade), acetonitrile (LC-MS grade), isopropanol (IPA) and formic acid (FA, 98% *v/v*) were purchased from Fluka (St. Louis, MO, USA). Distilled water was purified by a Milli-Q system (Milford, MA, USA). DNase I recombinant expressed by *Pichia pastoris* (R-DNase, 10,000 U/mg), phosphodiesterase-1 extracted from *Crotalus adamanteus* (PDE-1, 0.4 U/mg), recombinant alkaline phosphatase expressed by *Pichia pastoris* (R-ALP, 7,000 U/mg), and calf thymus DNA (CtDNA) were purchased from Roche (St. Louis, MO, USA). Single membrane filtration devices Microcon (10

kDa cutoff, 0.5 mL) were purchased from Amicon (Billerica, MA, USA). Silanized vials (0.3 mL, 1.2 mL and 4 mL) were purchased from ChromTech (Apple Valley, MN, USA). Internal standards [$^{15}N_5$]-*N*^{2}-ethyl-deoxyguanosine (dG) and [$^{15}N_5$]-*N*^{6}-methyl-deoxyadenosine (dA) were synthesized as described by Wang et al.[94,95]

^{15}N-DNA Generation. *Escherichia coli* (MG1655 strain) was cultured in ^{15}N-labeled minimal medium (5 mL) at 37 °C overnight, for three generations to obtain a uniformly labeled ^{15}N-strain. The OD_{600} was used to monitor bacterial growth until stationary phase. The bacteria culture was centrifuged at 3000×g for 10 min at 24 °C. The bacterial pellet was resuspended in 50% glycerol in bacterial medium solution, frozen and stored in −80 °C until use. ^{15}N-labeled minimal medium (1 L) was prepared using 200 mL of M9 salts (Na_2HPO_4•$7H_2O$, 64 g KH_2PO_4, 15 g, NaCl, 2.5 g, $^{15}NH_4Cl$, 5.0 g, deionized H_2O, to 1 L), 20 mL of glucose (20%; Sigma-Aldrich), 2 mL of $MgSO_4$ (1 M; Fisher Scientific), 100 µL of $CaCl_2$ (1 M; Fisher Scientific). A starter culture was done by inoculating 10 µL of ^{15}N and ^{14}N- stock bacteria into 5 mL of medium and grown overnight. 50 µL of cells were then inoculated in 1 L of medium and incubated overnight. Cells were centrifuged and pellet stored at -80 °C until use.

Bacterial ^{15}N-DNA Isolation. Cells were resuspended in 25 mL of Cell Lysis Solution (Qiagen) and treated with 150 µL of Proteinase-K (24 h, 24 °C) and RNase-A (2 h, 24 °C). Proteins were precipitated by adding 7.5 mL of Protein Precipitation Solution (Qiagen). The pellet was discarded and the supernatant was transferred into a new tube containing an equal amount of cold IPA to precipitate the DNA. The mixture was centrifuged, the supernatant was discarded and the DNA pellet washed with IPA 70 % v/v in water and then with 100% IPA. The pellets were dried, resuspended in DNA buffer (20 mM Tris, 2 mM $MgCl_2$ pH 7.4), and stored at -20

°C. The yield and purity of the DNA was assessed using a nanodrop UV/Vis spectrophotometer monitoring the 260 nm and 280 nm wavelengths.

DNA Exposure and Digestion. CtDNA (100 µg), bacterial DNA (100 µg), and ^{15}N-bacterial DNA (100 µg), were dissolved in Tris buffer (20 mM Tris, 2 mM $MgCl_2$ pH 7.4). Tilimycin and tilivalline were added to the DNA solutions separately (100 µM). The samples total volume was 200 µL and they were incubated at 37 °C overnight. DNA exposure to DMSO (1% v/v) was used as a negative control. DNA isolation was performed by IPA precipitation. Briefly, 1 mL of cold IPA was added to each sample vial. The precipitated DNA was isolated, washed twice with 1 mL 70% IPA and 1 mL 100% IPA and dried under a nitrogen stream. All steps of the protocol were performed using silanized glass vials.

DNA Isolation from HEK Cells. HEK293T cells in MEM media containing 10% FBS, 100 U/mL penicillin and 100 µg/mL streptomycin under a 5% CO_2 atmosphere at 37 °C were grown to 90% confluency in T75 flasks (Corning CLS3275; ~6 x 10^6 cells). The cells were then washed with PBS and incubated with 1 µM tilimycin or DMSO (0.2%) in FBS free MEM media for 24 h at 37 °C. Following treatment, the cells were washed PBS, suspended in a trypsin-containing buffer, pelleted at 500×g for 5 min, and further washed 3 times in PBS. Cells were resuspended in 15 mL of Cell Lysis Solution (Qiagen) and treated with 150 µL of Proteinase-K (24h, RT) and RNase-A (2 h, RT). Proteins were precipitated by adding 7.5 mL of Protein Precipitation Solution (Qiagen). The pellet was discarded and the supernatant was transferred into a new tube containing an equal amount of cold IPA to precipitate the DNA. The mixture was centrifuged and the supernatant was discarded and the DNA pellet washed with IPA 70 % v/v in water and then with 100% IPA. The pellets were dried, resuspended in appropriate buffer, and stored at -20

°C. The yield and purity of the DNA was assessed using a nanodrop UV/Vis spectrophotometer monitoring the 260 nm and the 280 nm wavelengths.

DNA Hydrolysis and Deoxyguanosine Quantitation via HPLC. DNA was enzymatically hydrolyzed. Recombinant-DNase was added (0.5 U/μg DNA) and the samples were incubated overnight at 24 °C. Then, Recombinant-DNase (0.5 U/μg DNA), R-ALP-1 (0.4U U/μg DNA) and PDE-1 (0.02 mU/μg DNA) were added and the samples were incubated at 37 °C for 2 h and additionally, overnight at 24 °C. Enzymes were removed before dG quantitation via filtration (Microcon, 10 kDa cutoff). The recovery of the DNA adducts was determined by spiking the samples with isotopically labeled internal standards ([$^{15}N_5$]-N^2-ethyl-dG and [$^{15}N_5$]-N^6-methyl-dA 100 fmol each).

Quantitation of dG was carried out with a Dionex UltiMate 3000 RSLCnano System (Thermo Scientific, Waltham, MA) with a UV detector set at 254 nm. A 300 μm ID × 15 cm C18 column (2 μm, 100 Å) (Thermo Scientific, Waltham, MA) was used with water (A) and CH_3OH (B) as mobile phases, an injection volume of 1 μL, and a flow rate of 15 μL/min. The elution gradient was as follows: an initial condition of 5% B for 2 min, a linear gradient from 2% to 25% B in 10 min, and then from 25% to 95% B in 3 min, followed by a 5 min hold, a return to the starting conditions over 2 min and re-equilibration for 3 min (25 min total run time). A calibration curve for dG (0.0625-50 ng/μL) was performed in triplicate. The amount of dG in each sample was calculated using the peak area, the slope of the calibration curve, and the fraction of the total volume injected. The amount of dG was then used to calculate the amount of DNA in each sample using the ratio of 1 mg of DNA per 0.66 μmol of dG.

Sample Enrichment and Purification. Samples were purified by solid-phase extraction using Strata-X cartridges (30 μm, Phenomenex, Torrance, CA) after washing with 3 mL of CH_3OH

and equilibrating with 1 mL of H_2O. The samples were loaded on the cartridges, washed with 1 mL of H_2O, and eluted with 1 mL of 10% CH_3OH, 100% CH_3OH and 2% formic acid in CH_3OH sequentially. The last two eluted fractions were evaporated to dryness and reconstituted in 2% CH_3OH/H_2O to a final volume of 20 µL.

LC Conditions for MS Analysis. The dried hydrolyzed DNA samples were reconstituted in 20 µL of 2% CH_3OH/H_2O (LC-MS grade, Fluka) and 1 µL analyzed by LC-MS. The LC was performed using a nanoflow UPLC (Ultimate 3000 RSLCnano UPLC, Thermo Scientific, Waltham, MA). The UPLC was equipped with a 5 µL loop and reversed-phase chromatographic separation was performed using a hand-packed commercially available fused-silica emitter (230 × 0.075 mm ID, 15 µm orifice, New Objective, Woburn MA) with C18 stationary phase (5 µm, 100, Luna Phenomenex, Torrance, CA). The mobile phase consisted of an aqueous solution of 0.05% (v/v) formic acid (A) and CH_3CN (B). The elution program included an isocratic step (2% of B for 5.5 min at 1 µL/min), followed by a two steps linear gradient of B (1.3%/min for 37 min and 24%/min for 2 min, both at 0.3 µL/min) and it concluded with a washing isocratic step, performed at 98% of B for 2 min at 0.3 µL/min. At the end of the elution program, the LC-system was equilibrated for 3 min at isocratic conditions (2% of B, 1 µL/min). The injection valve position was switched at 6 min to take the injection loop out of the flow path.

Mass Spectrometry. All mass spectrometry-based analysis was performed using a hybrid high-field Orbitrap mass spectrometer (Lumos, Thermo Scientific, Waltham, MA). The LC system was interfaced to the mass spectrometer using a Nanoflex ESI ion source (Nanoflex Thermo Scientific, Waltham, MA), which operated in positive ion mode at 2.5 kV. The transfer ion tube temperature was 300 °C, and S-Lens setting was 60.

Untargeted Adductomic Screening Analysis. The screening method was performed using a data dependent acquisition-constant neutral loss/MS^3 (DDA-CNL/MS^3) approach, consisting of full scanning with data dependent MS^2 and neutral loss MS^3 acquisition (NL-MS^3). The full scan (150–1,200 *m/z*) was performed with quadrupole filtering, maximum injection time of 50 ms, automatic gain control target of 2×10^5, and a resolution setting of 120,000. Data dependent parameters were: dynamic exclusion of 30 s, mass tolerance of ± 5 ppm, repeat count of 1, minimum intensity of 2×10^4, and a cycle time of 3 s. An MS^2 exclusion list of 18 masses (Table **S2**), consisting of unmodified nucleosides and their electrostatically bound dimer ions, was used with a mass tolerance of ± 5 ppm. MS^2 scan events were triggered based on an intensity threshold of 2×10^4. The MS^2 fragmentation was performed with a quadrupole isolation width of 1.5 *m/z*, stepped HCD collision energy (15, 25, 35%), AGC value of 2×10^5, maximum injection time of 54 ms, and Orbitrap detection at a resolution setting of 30,000. For the NL-MS^3 data acquisitions, MS^2 product ions were isolated in the ion trap with an isolation window of 2 *m/z*, and MS^3 fragmentation triggered upon observation of the neutral loss of the 2′-deoxyribose (dR) or the base moieties (-dR; 116.0474, -G; 151.0494, -A: 135.0545, -T; 126.0429; -C; 111.0433 ± 5 ppm), with HCD fragmentation (40%), Orbitrap detection at a resolution of 15,000, AGC value of 200,000 and a maximum injection time of 200 ms. A set of scan events was included for the targeted fragmentation of hypothesized ions of interest. 6 tilimycin derived-DNA adducts (484.1946 *m/z*, 468.1997 *m/z*, 368.1472 *m/z*, 352.1523 *m/z*, 459.1881 *m/z*, 444.1884 *m/z*), was investigated with quadrupole isolation widths of 1.5 *m/z*, maximum injection time of 54 ms, AGC of 200,000, and resolution setting of 30,000. Fragmentation was performed using HCD with stepped collision energy (16, 26, 36%). LC and injection conditions are as reported in the LC Conditions for MS Analysis section.

Targeted Adduct Analysis. The targeted adduct analysis was performed using targeted MS^2 analysis of 4 tilimycin derived-DNA adducts (484.1946 *m/z*, 468.1997 *m/z*, 368.1472 *m/z*, 352.1523 *m/z*), with quadrupole isolation widths of 1.5 *m/z*, maximum injection time of 246 ms, AGC of 1×10^6, and resolution setting of 120,000. Fragmentation was performed using HCD with a stepped collision energy (16, 26, 36%). The fragmentation of the DNA adduct precursor ions $[MH]^+$ results in neutral loss of the dR, G, A, T or C moiety to produce the corresponding $[MH\text{-}dR]^+$, $[MH\text{-}G]^+$, $[MH\text{-}A]^+$, $[MH\text{-}T]^+$, and $[MH\text{-}C]^+$ product ions whose masses are extracted for detection of the adducts. LC and injection conditions are as reported in LC Conditions for MS Analysis section.

Data Analysis. For DNA adduct screening data analysis, RawConverter (http://fields.scripps.edu/rawconv/) was used to convert the Thermo Scientific raw data files to mzXML files which were imported into a SQL database, where data filtration on the basis of MS^3 triggering ion *m/z* and retention time was performed. MS^3 triggering ions present in the exposed samples with both *m/z* (±5 ppm) and retention times (± 30 s) different than those in the control (non-exposed) samples, were selected and reported as putative DNA adducts. The absence of putative DNA adduct ion signals in the control samples were further confirmed by generating extracted ion chromatograms for all putative DNA adduct precursor masses at 5 ppm mass tolerance using the Qualbrowser component of the Xcalibur 3.0 software package (Thermo Scientific, Waltham, MA). MS^2 and MS^3 spectra of each putative DNA adduct were subsequently evaluated for structural information and the peak area of the precursor mass was determined. Ions uniquely found in exposed samples were then confirmed by manually searching the the corresponding ^{15}N-version of the hypothesized adduct in the ^{15}N-labelled-DNA sample.

MS^2 and MS^3 spectra of ^{15}N-molecules were also compared with the ones observed in unlabelled or cell-derived DNA.

General Methods for Chemistry. All commercial reagents (Sigma-Aldrich, Acros Organics, and Alfa-Aesar) were used as provided unless otherwise indicated. Compounds **2**[96], **6**[46], and **10**[97] were synthesized as described. ACS and HPLC grade solvents were purchased from Fischer Scientific. An anhydrous solvent dispensing system (MBRAUN) using packed columns of neutral alumina was used for drying CH_2Cl_2 and the solvents were dispensed under nitrogen. All reactions were performed under an inert atmosphere of argon in oven dried (130-150 °C) glassware. Thin layer chromatography (TLC plate, Merck EMD Millipore) was performed on a pre-coated silica gel 60 F254 plates. The detection of compounds was carried out with UV light. Flash chromatography was performed with silica gel P60 (Silicycle) with the indicated solvent system. All NMR spectra were recorded on a Varian 400 MHz spectrometer. ^1H NMR spectra were referenced to residual $CDCl_3$ (7.27 ppm) or CD_3OD (3.31 ppm); ^{13}C NMR spectra were referenced to $CDCl_3$ (77.23 ppm) or CD_3OD (49.0 ppm). Data for ^1H NMR are reported as follows: chemical shift (multiplicity, coupling constant in Hertz (Hz), number of hydrogens). Abbreviations are as follows: s = singlet, d = doublet, t = triplet, q = quartet, p = pentet, m = multiplet, br = broad. High-resolution mass spectra (HRMS) were obtained at the Department of Chemistry, University of Minnesota, on a Bruker BioTOF II instrument.

Synthesis of Tilimycin and Tilivalline Tilimycin, tilivalline and *O*-benzyltilivalline were synthesized as described and the ^1H NMR and HRMS data matched previously reported data.[29,98]

General Procedure 1: Global Deprotection. Fully protected adenosine acyl-sulfamide adenylate (**4, S3, S4**) (0.1 mmol) was dissolved in EtOH (20 mL), then charged with 5% *w/w* Pd/C (10 wt%). The flask was evacuated and backfilled with H_2 three times, then stirred under an

atmosphere of H_2 for 3 h. The Pd/C was removed by filtering through a pad of celite and the supernatant was concentrated to yield a waxy brown solid. The solid was dissolved in TFA:H_2O (4:1) and stirred at room temperature for an additional 3 h. The acidic solution was concentrated *in vacuo* to yield a crude orange solid. The crude material was redissolved (10 mg/mL) in 1:1 MeCN-50 mM triethylammonium bicarbonate (pH 7.5) and filtered to remove insoluble solids. The resulting solution was purified by preparative reverse phase HPLC with a Phenomenex Gemini C18 (250 mm × 21 mm) column at a flow rate of 21.0 mL/min employing a gradient of 5→30% acetonitrile (Solvent B) in 50 mM aqueous triethylammonium bicarbonate at pH 7.5 for 15 minutes. Fractions containing the product were pooled and lyophilized to afford the final compound as the triethylammonium salt.

5′-[*N*-Sulfamoyl]amino-2′,3′-*O*-isopropylidene-5′-deoxyadenosine (3). Compound **2** (690 mg, 2.08 mmol, 1 equiv) was dissolved in EtOH (15 mL). The flask was charged with 5% *w/w* Pd/C (70 mg, 10 wt%) evacuated and backfilled with H_2 three times, then stirred under an atmosphere of H_2 for 2 h. The Pd/C was removed by filtering through a pad of celite and the supernatant was concentrated to yield a yellow oil. The crude material was redissolved in 1,4 dioxanes (25 mL) and refluxed for 2 h. The reaction mixture was concentrated and purified by silica gel flash chromatography (dry loading, 1→5% MeOH/EtOAc) affording the title compound (510 mg, 64%) as a white solid: R_f = 0.24 (5:95 MeOH/EtOAc); ^{1}H NMR (400 MHz, CD_3OD) δ 1.36 (s, 3H), 1.60 (s, 3H), 3.36 (dd, 2H, *J* = 3.90, 5.24 Hz), 4.47 (td, 1H, *J* = 2.32, 3.78, 3.78 Hz), 5.09 (dd, 1H, *J* = 2.45, 6.23 Hz), 5.32 (dd, 1H, *J* = 4.10, 6.26 Hz), 6.05 (d, 1H, *J* = 4.07 Hz), 8.22 (s, 1H), 8.26 (s, 1H). MS (ESI+) *m/z* calcd for $C_{13}H_{19}N_7O_5SNa$+ $[M+Na]^+$ 408.1, found 408.6.

5′-[*N*-(3-Benzyloxy-2-nitrobenzoyl)sulfamoyl]amino-2′,3′-*O*-isopropylidene-5′-deoxyadenosine (4). The NHS-ester **7** (74 mg, 0.2 mmol, 1.5 equiv) and adenosine

monosulfamide (**3**) (50 mg, 0.13 mmol, 1 equiv) were dissolved in DMF (5 mL). The reaction mixture was cooled to 0 °C and Cs_2CO_3 (130 mg, 0.4 mmol, 3 equiv) was added. The reaction was allowed to warm to room temperature and stirred for 18 h. The excess Cs_2CO_3 was removed by filtration with a sintered glass filter and the supernatant was concentrated to yield a yellow solid, which was purified by silica gel flash chromatography (dry loading, 2.5→15% MeOH/EtOAc) afforded the title compound (53 mg, 65%) as a white solid: R_f = 0.25 (10:90 MeOH/EtOAc); ^{1}H NMR (400 MHz, CD_3OD) δ 1.32 (s, 3H), 1.56 (s, 3H), 3.35–3.37 (m, 2H), 4.41–4.42 (m, 1H), 5.08 (dd, *J* = 6.1, 2.5 Hz, 1H), 5.16 (s, 2H), 5.32 (dd, *J* = 6.2, 3.8 Hz, 1H), 6.07 (d, *J* = 3.7 Hz, 1H), 7.25–7.39 (m, 8H), 8.23 (s, 1H), 8.26 (s, 1H); ^{13}C NMR (100 MHz, CD_3OD) δ 25.6, 27.6, 46.3, 72.2, 83.4, 84.7, 85.7, 92.4, 115.6, 117.7, 120.6, 122.5, 128.3, 129.1, 129.14, 129.5, 131.8, 133.3, 137.3, 141.7, 150.0, 151.0, 154.0, 157.2, 170.3; HRMS (ESI–) *m/z* calcd for $C_{27}H_{27}N_8O_9S^-$ $[M–H]^–$ 639.1627, found 639.1657 (error 4.5 ppm).

5′-[*N*-(2-Amino-3-hydroxybenzoyl)sulfamoyl]amino-5′-deoxyadenosine triethylammonium salt (5). The title compound was prepared from **4** using general procedure 1 to afford a colorless foam (20 mg. 45%): HPLC purity = 93.8%, t_R = 8.86 min, k' = 2.5; ^{1}H NMR (400 MHz, CD_3OD) δ 1.29 (t, *J* = 8 Hz, 27 H, excess Et_3N), 3.16 (q, *J* = 8 Hz, 18 H, excess Et_3N), 3.29–3.41 (m, 2H), 4.26 (q, *J* = 3.4 Hz, 1H), 4.35 (dd, *J* = 5.4, 2.5 Hz, 1H), 4.86–4.90 (m, 1H), 5.91 (d, *J* = 6.8 Hz, 1H), 6.47 (t, *J* = 7.9, 1H), 6.76 (d, *J* = 7.7 Hz, 1H), 7.23 (d, *J* = 8.1 Hz, 1H), 8.26 (s, 1H), 8.39 (s, 1H), 8.55 (s, 2H); ^{13}C NMR (100 MHz, CD_3OD) δ 9.3, 46.5, 47.8, 73.2, 74.6, 85.9, 91.0, 115.1, 115.9, 119.5, 120.2, 138.7, 140.7, 145.2, 148.8, 152.7, 155.7, 171.8; HRMS (ESI–) *m/z* calcd for $C_{17}H_{19}N_8O_7S^-$ $[M–H]^–$ 479.1103, found 479.1088 (error 3.6 ppm).

3-Benzyloxy-2-nitrobenzoic acid *N*-hydroxysuccinimide ester (7). Aryl acid **6**[46] (270 mg, 1 mmol, 1 equiv) was dissolved in THF (25 mL). The solution was cooled to 0 °C. *N*-

hydroxysuccimide (250 mg, 2.2 mmol, 2.2 equiv) was added followed by DCC (450 mg, 2.2 mmol, 2.2 equiv). The reaction mixture was allowed to warm to room temperature and stirred for 12 h. The resulting precipitate was filtered with a sintered glass filter and the supernatant was concentrated and purified by silica gel flash chromatography (dry loading, 10→50% EtOAc/hexanes) affording the title compound (315 mg, 85%) as a white solid: R_f = 0.30 (50:50 EtOAc/hexanes); ^{1}H NMR (400 MHz, $CDCl_3$) δ 2.88 (s, 4H), 5.24 (s, 2H), 7.33–7.40 (m, 6H), 7.51 (t, J = 8.19 Hz, 1H), 7.76 (d, J = 7.86 Hz, 1H); ^{13}C NMR (100 MHz, $CDCl_3$) δ 25.8, 71.7, 118.7, 121.0, 122.8, 127.2, 128.7, 129.0, 131.2, 134.8, 150.5, 158.5, 168.6 (missing 1 aryl carbon); HRMS (ESI+) *m/z* calcd for $C_{18}H_{14}N_2O_7Na^+$ $[M+Na]^+$ 393.0693, found 393.0692 (error 0.4 ppm).

5′-[*N*-(3-Hydroxybenzoyl)sulfamoyl]amino-5′-deoxyadenosine triethylammonium salt (8). The title compound was prepared from **S3** using general procedure 1 afford a colorless foam (23 mg, 49%): HPLC purity = 99.8%, t_R = 12.10 min, k' = 3.5; ^{1}H NMR (400 MHz, CD_3OD) δ 1.27 (t, J = 8.0 Hz, 9H), 3.15 (q, J = 8.0 Hz, 6H), 3.31–3.35 (m, 2H), 4.24 (q, J = 3.4 Hz, 1H), 4.34–4.36 (dd, J = 5.4, 2.8 Hz, 1H), 4.85–4.86 (m, 1H), 5.92 (d, J = 6.5 Hz, 1H), 6.87 (d, J = 2.6 Hz, 1H), 7.18 (t, J = 7.9 Hz, 1H), 7.38 (s, 1H), 7.43 (d, J = 7.9 Hz, 1H), 8.28 (s, 1H), 8.33 (s, 1H); ^{13}C NMR (100 MHz, CD_3OD) δ 9.3, 46.4, 47.8, 73.1, 74.8, 85.9, 90.7, 116.3, 119.3, 120.7, 120.8, 129.9, 139.5, 141.9, 150.4, 154.2, 157.4, 158.3 (missing 1 aryl carbon); HRMS (ESI–) *m/z* calcd for $C_{17}H_{18}N_7O_7S^-$ $[M–H]^–$ 464.0994, found 464.0978 (error 3.4 ppm).

5′-[*N*-(2-Aminobenzoyl)sulfamoyl]amino-5′-deoxyadenosine triethylammonium salt (9). The title compound was prepared from **S4** using general procedure 1 to afford a colorless foam (12 mg, 25%): HPLC purity = 90.5%, t_R = 9.98 min, k' = 2.9; ^{1}H NMR (400 MHz, CD_3OD) δ 1.23 (t, J = 8.0 Hz, 9H), 3.05 (q, J = 8.0 Hz, 6H), 3.31–3.34 (m, 2H), 4.24 (q, J = 3.3 Hz, 1H), 4.36 (dd,

J = 5.4, 2.9 Hz, 1H), 4.82–4.85 (m, 1H), 5.94 (d, *J* = 6.3 Hz, 1H), 6.56 (t, *J* = 7.5, 1H), 6.67 (d, *J* = 8.2 Hz, 1H), 7.10 (t, *J* = 8.3 Hz, 1H), 7.80 (d, *J* = 8.0 Hz, 1H), 8.31 (s, 2H); ^{13}C NMR (100 MHz, CD_3OD) δ 9.6, 46.5, 47.7, 73.0, 74.9, 85.9, 90.4, 117.0, 118.0, 120.5, 120.7, 131.8, 132.8, 141.8, 150.5, 150.7, 154.1, 157.3, 175.9; HRMS (ESI–) *m/z* calcd for $C_{17}H_{19}N_8O_6S^-$ $[M–H]^–$ 463.1154, found 463.1130 (error 5.0 ppm).

***(E)-tert*-Butyl {2-[3-(methoxymethoxy)phenyl]ethenyl}sulfonylcarbamate (11)** *tert*-Butyl[(diphenylphosphoryl)methyl]sulfonyl carbamate[49] (150 mg, 0.37 mmol, 1 equiv) was dissolved in DMF (5 mL) under an atmosphere of argon. The solution was cooled to 0 °C and NaH (27 mg, 1.1 mmol, 3 equiv) was added. The reaction mixture was allowed to warm to 24 °C and stirred for an additional 30 min to ensure complete conversion to the ylide. Aldehyde **10**[97] (63 mg, 0.37 mmol, 1 equiv) was added as a solution in DMF (2 mL) and the reaction was stirred overnight. The reaction mixture was concentrated to a yellow oil and partitioned between H_2O (20 mL) and EtOAc (20 mL). The organic layer was collected, dried over Na_2SO_4 and concentrated to a light-yellow oil. Purification by flash chromatography (15→30% EtOAc/Hexanes) afforded the title compound (120 mg, 92%) as a white solid: R_f = 0.45 (33:67 EtOAc/Hexanes); ^{1}H NMR (400 MHz, $CDCl_3$) δ 1.85 (s, 9H), 3.50 (s, 3H), 5.21 (s, 2H), 5.30 (s, 1H), 6.99 (d, *J* = 15.5 Hz, 1H), 7.13–7.18 (m, 2H), 7.21 (s, 1H), 7.35 (t, *J* = 8.0 Hz, 1H), 7.64 (d, *J* = 15.5 Hz, 1H); ^{13}C NMR (100 MHz, $CDCl_3$) δ 28.1, 56.2, 84.3, 94.6, 116.0, 119.5, 122.5, 124.5, 130.3, 133.6, 144.4, 149.6, 157.9; HRMS (ESI+) *m/z* calcd for $C_{15}H_{22}NO_6S^+$ $[M+H]^+$ 344.1162, found 344.1101 (error 1.6 ppm).

(*E*)-5′-Deoxy-5′-*N*-*tert*-butoxycarbonyl-2′,3′-*O*-isopropylidene-5′-*N*-({2-[3-(methoxymethoxy)phenyl]ethenyl}sulfonyl)adenosine (12) To a solution of 2′,3′-*O*-isopropylideneadenosine **1** (32 mg, 0.1 mmol), **11** (30 mg, 0.09 mmol) and triphenylphosphine

(34 mg, 0.13 mmol), in THF (1 mL) at 0 °C was added a solution of DIAD (26 μL, 0.13 mmol) in THF (1 mL) over 10 min. The solution was allowed to warm to 24 °C and stirred for 15 h. The mixture was concentrated and purified by flash chromatography (100% EtOAc) to afford a white foam (10 mg, 75% brsm): R_f = 0.12 (100% EtOAc); ^{1}H NMR (400 MHz, CD_3OD) δ 1.38 (s, 3H), 1.41 (s, 9H), 1.58 (s, 3H), 3.46 (s, 3H), 4.03–4.06 (m, 2H), 4.44–4.48 (m, 1H), 5.18 (dd, *J* = 6.4, 3.3 Hz, 1 H), 5.23 (s, 2H), 5.52 (d, 6.3 Hz, 1H), 6.25 (d, *J* = 2.0 Hz, 1H), 7.02 (d, *J* = 15.4 Hz, 1H), 7.12 (t, *J* = 9.5 Hz, 1H), 7.18 (s, 1H), 7.34 (t, *J* = 8.0 Hz, 1H), 7.36 (d, *J* = 15.5 Hz, 1H), 8.23 (s, 1H), 8.27 (s, 1H). MS (ESI+) *m/z* calcd for $C_{28}H_{37}N_6O_9S^+$ $[M+H]^+$ 633.2, found 633.3.

(*E*)-5′-Amino-5′-deoxy-5′-*N*-{[2-3-hydroxyphenyl)ethenyl]sulfonyl}adenosine (13) To a solution of **12** (7 mg, 0.01 mmol) was added 80% aqueous TFA (5 mL). The solution was stirred at 24 °C for 2 h then concentrated. Purification by flash chromatography (1→10% MeOH/EtOAc) afforded a white solid (5 mg, 95%): HPLC purity = 94.1%, t_R = 11.97 min, k' = 3.6 R_f = 0.30 (1:9 MeOH/EtOAc); ^{1}H NMR (600 MHz, CD_3OD) δ 3.41 (d, *J* = 3.5 Hz, 1H), 4.28 (q, *J* = 3.2 Hz, 1H), 4.37 (dd, *J* = 5.4, 2.7 Hz, 1H), 4.87-4.89 (m, 1H), 5.93 (d, *J* = 6.6 Hz, 1H), 6.85 (dd, *J* = 8.2, 2.5 Hz), 6.95 (d, *J* = 15.4 Hz, 1H), 6.97 (s, 1H), 7.02 (d, *J* = 7.6 Hz, 1H), 7.22 (t, *J* = 7.9 Hz, 1H), 7.37 (d, *J* = 15.4 Hz, 1H), 8.24 (s, 1H), 8.26 (s, 1H); ^{13}C NMR (100 MHz, CD_3OD) δ 45.8, 73.0, 74.4, 85.9, 91.5, 115.5, 118.9, 120.8, 121.2, 126.7, 131.1, 135.5, 142.2, 142.3, 150.0, 153.7, 157.6, 159.2; HRMS (ESI+) *m/z* calcd for $C_{18}H_{21}N_6O_6S^+$ $[M+H]^+$ 449.1237, found 449.1230 (error 1.6 ppm).

ASSOCIATED CONTENT

Supporting Information: The Supporting Information is available free of charge via the Internet at http://pubs.acs.org. A complete list of LC-MS/MS parameters and fragmentation data, X-ray crystallographic data for NpsA and ThdA and ^{1}H and ^{13}C NMR of all compounds.

AUTHOR INFORMATION

*For C.C.A. phone 612-624-7997. Fax 612-626-3114. Email: aldri015@umn.edu; A.M.G. phone 716-829-3696. Email: amgulick@buffalo.edu

Author Contributions. The manuscript was written with contributions of all authors. All authors have given approval to the final version of the manuscript.

Notes

The authors declare no competing financial interests.

ACKNOWLEDGMENTS

This work was supported by grants (GM116957 and GM136235 to A.M.G.) from the National Institutes of Health. Mass spectrometry for tilivalline quantitation was carried out in the Center for Mass Spectrometry and Proteomics Mass spectrometry for DNA adductomics was carried out in the Analytical Biochemistry Shared Resource of the Masonic Cancer Center, University of Minnesota and supported in part by the U.S. National Institutes of Health and National Cancer Institute (Cancer Center Support Grant CA-77598). Isothermal titration calorimetry was carried out using an ITC-200 microcalorimeter, funded by the NIH Shared Instrumentation Grant S10-OD017982. GM/CA@APS has been funded in whole or in part with Federal funds from the National Cancer Institute (ACB-12002) and the National Institute of General Medical Sciences (AGM-12006). This research used resources of the Advanced Photon Source, a U.S. Department

of Energy (DOE) Office of Science User Facility operated for the DOE Office of Science by Argonne National Laboratory under Contract No. DE-AC02-06CH11357. Use of the Stanford Synchrotron Radiation Lightsource, SLAC National Accelerator Laboratory, is supported by the U.S. Department of Energy, Office of Science, Office of Basic Energy Sciences under Contract No. DE-AC02-76SF00515. The SSRL Structural Molecular Biology Program is supported by the DOE Office of Biological and Environmental Research, and by the National Institutes of Health, National Institute of General Medical Sciences (P41GM103393).

ABBREVIATIONS

3HA-AMP, 3-hydroxyanthraniloyl adenosine monophosphate; A_{sub}, adenylation domain C-terminal subdomain; AAHC, antibiotic associated hemorrhagic colitis; ACP, acyl-carrier protein; acyl-AMS, acyl adenosine monosulfamide; ATP, adenosine triphosphate; AVS, adenosine vinylsulfonamide; CASO, tryptic soy broth; ctDNA, calf thymus DNA; dG, 2'-deoxyguanosine; dA, 2;-deoxyadenosine; ΔG, gibbs free energy; GI, gastrointestinal; ΔH, enthalpy; HPLC, high performance liquid chromatography; IMAC, immobilized metal affinity chromatography; ITC, isothermal titration calorimetry; K_D dissociation constant; LC-MS, liquid chromatography-mass spectrometry; LC-MS/MS, liquid chromatography-tandem mass spectrometry; L-Pro-S~T_{NpsB} prolyl-loaded thiolation domain; NHS, *N*-hydroxysuccinimidyl; NL, neutral loss; NRPS, nonribosomal peptide synthetase; MDFF, molecular dynamics flexible fitting; MEM, Dulbecco's minimum essential medium; MesG, 7-methylthioguanine; PBD, pyrrolobenzodiazepine; PPi, pyrophosphate; ΔS, entropy; SEC, size exclusion chromatography; SER, surface entropy reduction; *sfp,* 4'-phosphopantetheinyl transferase; TEV, tobacco etch virus.

References

(1) Savage, D. C. (1977) Microbial Ecology of the Gastrointestinal Tract. *Annu. Rev. Microbiol. 31*, 107–133.

(2) Eloe-Fadrosh, E. A., and Rasko, D. A. (2013) The Human Microbiome: From Symbiosis to Pathogenesis. *Annu. Rev. Med. 64*, 145–163.

(3) Nougayrede, J.-P. (2006) Escherichia coli Induces DNA Double-Strand Breaks in Eukaryotic Cells. *Science 313*, 848–851.

(4) Peery, A. F., Dellon, E. S., Lund, J., Crockett, S. D., McGowan, C. E., Bulsiewicz, W. J., Gangarosa, L. M., Thiny, M. T., Stizenberg, K., Morgan, D. R., Ringel, Y., Kim, H. P., DiBonaventura, M. D., Carroll, C. F., Allen, J. K., Cook, S. F., Sandler, R. S., Kappelman, M. D., and Shaheen, N. J. (2012) Burden of Gastrointestinal Disease in the United States: 2012 Update. *Gastroenterology 143*, 1179-1187.e3.

(5) Belizário, J. E., and Napolitano, M. (2015) Human microbiomes and their roles in dysbiosis, common diseases, and novel therapeutic approaches. *Front. Microbiol. 6*.

(6) Marchesi, J. R., Adams, D. H., Fava, F., Hermes, G. D. A., Hirschfield, G. M., Hold, G., Quraishi, M. N., Kinross, J., Smidt, H., Tuohy, K. M., Thomas, L. V., Zoetendal, E. G., and Hart, A. (2016) The gut microbiota and host health: a new clinical frontier. *Gut 65*, 330–339.

(7) Lynch, S. V., and Pedersen, O. (2016) The Human Intestinal Microbiome in Health and Disease. *N. Engl. J. Med.* (Phimister, E. G., Ed.) *375*, 2369–2379.

(8) Lloyd-Price, J., Abu-Ali, G., and Huttenhower, C. (2016) The healthy human microbiome. *Genome Med. 8*.

(9) Huttenhower, C., Gevers, D., Knight, R., Abubucker, S., Badger, J. H., Chinwalla, A. T., Creasy, H. H., Earl, A. M., FitzGerald, M. G., Fulton, R. S., Giglio, M. G., Hallsworth-Pepin, K., Lobos, E. A., Madupu, R., Magrini, V., Martin, J. C., Mitreva, M., Muzny, D. M., Sodergren, E. J., Versalovic, J., Wollam, A. M., Worley, K. C., Wortman, J. R., Young, S. K., Zeng, Q., Aagaard, K. M., Abolude, O. O., Allen-Vercoe, E., Alm, E. J., Alvarado, L., Andersen, G. L., Anderson, S., Appelbaum, E., Arachchi, H. M., Armitage, G., Arze, C. A., Ayvaz, T., Baker, C. C., Begg, L., Belachew, T., Bhonagiri, V., Bihan, M., Blaser, M. J., Bloom, T., Bonazzi, V., Paul Brooks, J., Buck, G. A., Buhay, C. J., Busam, D. A., Campbell, J. L., Canon, S. R., Cantarel, B. L., Chain, P. S. G., Chen, I.-M. A., Chen, L., Chhibba, S., Chu, K., Ciulla, D. M., Clemente, J. C., Clifton, S. W., Conlan, S., Crabtree, J., Cutting, M. A., Davidovics, N. J., Davis, C. C., DeSantis, T. Z., Deal, C., Delehaunty, K. D., Dewhirst, F. E., Deych, E., Ding, Y., Dooling, D. J., Dugan, S. P., Michael Dunne, W., Scott Durkin, A., Edgar, R. C., Erlich, R. L., Farmer, C. N., Farrell, R. M., Faust, K., Feldgarden, M., Felix, V. M., Fisher, S., Fodor, A. A., Forney, L. J., Foster, L., Di Francesco, V., Friedman, J., Friedrich, D. C., Fronick, C. C., Fulton, L. L., Gao, H., Garcia, N., Giannoukos, G., Giblin, C., Giovanni, M. Y., Goldberg, J. M., Goll, J., Gonzalez, A., Griggs, A., Gujja, S., Kinder Haake, S., Haas, B. J., Hamilton, H. A., Harris, E. L., Hepburn, T. A., Herter, B., Hoffmann, D. E., Holder, M. E., Howarth, C., Huang, K. H., Huse, S. M., Izard, J., Jansson, J. K., Jiang, H., Jordan, C., Joshi, V., Katancik, J. A., Keitel, W. A., Kelley, S. T., Kells, C., King, N. B., Knights, D., Kong, H. H., Koren, O., Koren, S., Kota, K. C., Kovar, C. L., Kyrpides, N. C., La Rosa, P. S., Lee, S. L., Lemon, K.

P., Lennon, N., Lewis, C. M., Lewis, L., Ley, R. E., Li, K., Liolios, K., Liu, B., Liu, Y., Lo, C.-C., Lozupone, C. A., Dwayne Lunsford, R., Madden, T., Mahurkar, A. A., Mannon, P. J., Mardis, E. R., Markowitz, V. M., Mavromatis, K., McCorrison, J. M., McDonald, D., McEwen, J., McGuire, A. L., McInnes, P., Mehta, T., Mihindukulasuriya, K. A., Miller, J. R., Minx, P. J., Newsham, I., Nusbaum, C., O'Laughlin, M., Orvis, J., Pagani, I., Palaniappan, K., Patel, S. M., Pearson, M., Peterson, J., Podar, M., Pohl, C., Pollard, K. S., Pop, M., Priest, M. E., Proctor, L. M., Qin, X., Raes, J., Ravel, J., Reid, J. G., Rho, M., Rhodes, R., Riehle, K. P., Rivera, M. C., Rodriguez-Mueller, B., Rogers, Y.-H., Ross, M. C., Russ, C., Sanka, R. K., Sankar, P., Fah Sathirapongsasuti, J., Schloss, J. A., Schloss, P. D., Schmidt, T. M., Scholz, M., Schriml, L., Schubert, A. M., Segata, N., Segre, J. A., Shannon, W. D., Sharp, R. R., Sharpton, T. J., Shenoy, N., Sheth, N. U., Simone, G. A., Singh, I., Smillie, C. S., Sobel, J. D., Sommer, D. D., Spicer, P., Sutton, G. G., Sykes, S. M., Tabbaa, D. G., Thiagarajan, M., Tomlinson, C. M., Torralba, M., Treangen, T. J., Truty, R. M., Vishnivetskaya, T. A., Walker, J., Wang, L., Wang, Z., Ward, D. V., Warren, W., Watson, M. A., Wellington, C., Wetterstrand, K. A., White, J. R., Wilczek-Boney, K., Wu, Y., Wylie, K. M., Wylie, T., Yandava, C., Ye, L., Ye, Y., Yooseph, S., Youmans, B. P., Zhang, L., Zhou, Y., Zhu, Y., Zoloth, L., Zucker, J. D., Birren, B. W., Gibbs, R. A., Highlander, S. K., Methé, B. A., Nelson, K. E., Petrosino, J. F., Weinstock, G. M., Wilson, R. K., and White, O. (2012) Structure, function and diversity of the healthy human microbiome. *Nature 486*, 207–214.

(10) Hajishengallis, G., and Lamont, R. J. (2016) Dancing with the Stars: How Choreographed Bacterial Interactions Dictate Nososymbiocity and Give Rise to Keystone Pathogens, Accessory Pathogens, and Pathobionts. *Trends Microbiol. 24*, 477–489.

(11) Petersen, C., and Round, J. L. (2014) Defining dysbiosis and its influence on host immunity and disease: How changes in microbiota structure influence health. *Cell. Microbiol. 16*, 1024–1033.

(12) Sampson, T. R., Debelius, J. W., Thron, T., Janssen, S., Shastri, G. G., Ilhan, Z. E., Challis, C., Schretter, C. E., Rocha, S., Gradinaru, V., Chesselet, M.-F., Keshavarzian, A., Shannon, K. M., Krajmalnik-Brown, R., Wittung-Stafshede, P., Knight, R., and Mazmanian, S. K. (2016) Gut Microbiota Regulate Motor Deficits and Neuroinflammation in a Model of Parkinson's Disease. *Cell 167*, 1469-1480.e12.

(13) Kowalski, K., and Mulak, A. (2019) Brain-Gut-Microbiota Axis in Alzheimer's Disease. *J. Neurogastroenterol. Motil. 25*, 48–60.

(14) Haran, J. P., Bhattarai, S. K., Foley, S. E., Dutta, P., Ward, D. V., Bucci, V., and McCormick, B. A. (2019) Alzheimer's Disease Microbiome Is Associated with Dysregulation of the Anti-Inflammatory P-Glycoprotein Pathway. *mBio* (Pettigrew, M. M., Ed.) *10,* e00632-19.

(15) Pickard, J. M., Zeng, M. Y., Caruso, R., and Núñez, G. (2017) Gut microbiota: Role in pathogen colonization, immune responses, and inflammatory disease. *Immunol. Rev. 279*, 70–89.

(16) Cani, P. D., Bibiloni, R., Knauf, C., Waget, A., Neyrinck, A. M., Delzenne, N. M., and Burcelin, R. (2008) Changes in Gut Microbiota Control Metabolic Endotoxemia-Induced

Inflammation in High-Fat Diet-Induced Obesity and Diabetes in Mice. *Diabetes 57*, 1470–1481.

(17) Qin, J., Li, Y., Cai, Z., Li, S., Zhu, J., Zhang, F., Liang, S., Zhang, W., Guan, Y., Shen, D., Peng, Y., Zhang, D., Jie, Z., Wu, W., Qin, Y., Xue, W., Li, J., Han, L., Lu, D., Wu, P., Dai, Y., Sun, X., Li, Z., Tang, A., Zhong, S., Li, X., Chen, W., Xu, R., Wang, M., Feng, Q., Gong, M., Yu, J., Zhang, Y., Zhang, M., Hansen, T., Sanchez, G., Raes, J., Falony, G., Okuda, S., Almeida, M., LeChatelier, E., Renault, P., Pons, N., Batto, J.-M., Zhang, Z., Chen, H., Yang, R., Zheng, W., Li, S., Yang, H., Wang, J., Ehrlich, S. D., Nielsen, R., Pedersen, O., Kristiansen, K., and Wang, J. (2012) A metagenome-wide association study of gut microbiota in type 2 diabetes. *Nature 490*, 55–60.

(18) Davis-Richardson, A. G., and Triplett, E. W. (2015) A model for the role of gut bacteria in the development of autoimmunity for type 1 diabetes. *Diabetologia 58*, 1386–1393.

(19) Xue, M., Kim, C. S., Healy, A. R., Wernke, K. M., Wang, Z., Frischling, M. C., Shine, E. E., Wang, W., Herzon, S. B., and Crawford, J. M. (2019) Structure elucidation of colibactin and its DNA cross-links. *Science 365*, eaax2685.

(20) De Angelis, M., Francavilla, R., Piccolo, M., De Giacomo, A., and Gobbetti, M. (2015) Autism spectrum disorders and intestinal microbiota. *Gut Microbes 6*, 207–213.

(21) Louis, P., Hold, G. L., and Flint, H. J. (2014) The gut microbiota, bacterial metabolites and colorectal cancer. *Nat. Rev. Microbiol. 12*, 661–672.

(22) Vizcaino, M. I., and Crawford, J. M. (2015) The colibactin warhead crosslinks DNA. *Nat. Chem. 7*, 411–417.

(23) Högenauer, C., Lippe, I. T., Krause, R., and Hinterleitner, T. A. (2006) Klebsiella oxytoca as a Causative Organism of Antibiotic-Associated Hemorrhagic Colitis. *N. Engl. J. Med.* 9.

(24) Schneditz, G., Rentner, J., Roier, S., Pletz, J., Herzog, K. A. T., Bucker, R., Troeger, H., Schild, S., Weber, H., Breinbauer, R., Gorkiewicz, G., Hogenauer, C., and Zechner, E. L. (2014) Enterotoxicity of a nonribosomal peptide causes antibiotic-associated colitis. *Proc. Natl. Acad. Sci. 111*, 13181–13186.

(25) Youn, Y., Lee, S. W., Cho, H.-H., Park, S., Chung, H.-S., and Seo, J. W. (2018) Antibiotics-Associated Hemorrhagic Colitis Caused by Klebsiella oxytoca: Two Case Reports. *Pediatr. Gastroenterol. Hepatol. Nutr. 21*, 141–146.

(26) Darby, A., Lertpiriyapong, K., Sarkar, U., Seneviratne, U., Park, D. S., Gamazon, E. R., Batchelder, C., Cheung, C., Buckley, E. M., Taylor, N. S., Shen, Z., Tannenbaum, S. R., Wishnok, J. S., and Fox, J. G. (2014) Cytotoxic and Pathogenic Properties of Klebsiella oxytoca Isolated from Laboratory Animals. *PLoS ONE* (Bereswill, S., Ed.) *9*, e100542.

(27) Dornisch, E., Pletz, J., Glabonjat, R. A., Martin, F., Lembacher-Fadum, C., Neger, M., Högenauer, C., Francesconi, K., Kroutil, W., Zangger, K., Breinbauer, R., and Zechner, E. L. (2017) Biosynthesis of the Enterotoxic Pyrrolobenzodiazepine Natural Product Tilivalline. *Angew. Chem. Int. Ed. 56*, 14753–14757.

(28) von Tesmar, A., Hoffmann, M., Abou Fayad, A., Hüttel, S., Schmitt, V., Herrmann, J., and Müller, R. (2018) Biosynthesis of the *Klebsiella oxytoca* Pathogenicity Factor Tilivalline:

Heterologous Expression, *in Vitro* Biosynthesis, and Inhibitor Development. *ACS Chem. Biol. 13*, 812–819.

(29) Tse, H., Gu, Q., Sze, K.-H., Chu, I. K., Kao, R. Y.-T., Lee, K.-C., Lam, C.-W., Yang, D., Tai, S. S.-C., Ke, Y., Chan, E., Chan, W.-M., Dai, J., Leung, S.-P., Leung, S.-Y., and Yuen, K.-Y. (2017) A tricyclic pyrrolobenzodiazepine produced by *Klebsiella oxytoca* is associated with cytotoxicity in antibiotic-associated hemorrhagic colitis. *J. Biol. Chem. 292*, 19503–19520.

(30) Hering, N. A., Fromm, A., Bücker, R., Gorkiewicz, G., Zechner, E., Högenauer, C., Fromm, M., Schulzke, J.-D., and Troeger, H. (2019) Tilivalline- and Tilimycin-Independent Effects of Klebsiella oxytoca on Tight Junction-Mediated Intestinal Barrier Impairment. *Int. J. Mol. Sci. 20*, 5595.

(31) Mohr, N., and Budzikiewicz, H. (1982) Tilivalline, a New Pyrrolo[2, 1-c][1, 4]Benzodiazepine Metabolite From Klebsiella. *Tetrahedron 38*, 147–152.

(32) Minami, J., Okabe, A., Shiode, J., and Hayashi, H. (1989) Production of a unique cytotoxin by Klebsiella oxytoca. *Microb. Pathog. 7*, 203–211.

(33) Unterhauser, K., Pöltl, L., Schneditz, G., Kienesberger, S., Glabonjat, R. A., Kitsera, M., Pletz, J., Josa-Prado, F., Dornisch, E., Lembacher-Fadum, C., Roier, S., Gorkiewicz, G., Lucena, D., Barasoain, I., Kroutil, W., Wiedner, M., Loizou, J. I., Breinbauer, R., Díaz, J. F., Schild, S., Högenauer, C., and Zechner, E. L. (2019) *Klebsiella oxytoca* enterotoxins tilimycin and tilivalline have distinct host DNA-damaging and microtubule-stabilizing activities. *Proc. Natl. Acad. Sci. 116*, 3774–3783.

(34) Fischbach, M. A., and Walsh, C. T. (2006) Assembly-Line Enzymology for Polyketide and Nonribosomal Peptide Antibiotics: Logic, Machinery, and Mechanisms. *Chem. Rev. 106*, 3468–3496.

(35) Kuhn, M. L., Alexander, E., Minasov, G., Page, H. J., Warwrzak, Z., Shuvalova, L., Flores, K. J., Wilson, D. J., Shi, C., Aldrich, C. C., and Anderson, W. F. (2016) Structure of the Essential *Mtb* FadD32 Enzyme: A Promising Drug Target for Treating Tuberculosis. *ACS Infect. Dis. 2*, 579–591.

(36) Drake, E. J., Duckworth, B. P., Neres, J., Aldrich, C. C., and Gulick, A. M. (2010) Biochemical and Structural Characterization of Bisubstrate Inhibitors of BasE, the Self-Standing Nonribosomal Peptide Synthetase Adenylate-Forming Enzyme of Acinetobactin Synthesis,. *Biochemistry 49*, 9292–9305.

(37) Gulick, A. M. (2009) Conformational Dynamics in the Acyl-CoA Synthetases, Adenylation Domains of Non-ribosomal Peptide Synthetases, and Firefly Luciferase. *ACS Chem. Biol. 4*, 811–827.

(38) Webb, M. R. (1992) A continuous spectrophotometric assay for inorganic phosphate and for measuring phosphate release kinetics in biological systems. *Proc. Natl. Acad. Sci. 89*, 4884–4887.

(39) Ehmann, D. E., Shaw-Reid, C. A., Losey, H. C., and Walsh, C. T. (2000) The EntF and EntE adenylation domains of Escherichia coli enterobactin synthetase: Sequestration and selectivity in acyl-AMP transfers to thiolation domain cosubstrates. *Proc. Natl. Acad. Sci. 97*, 2509–2514.

(40) Wilson, D. J., and Aldrich, C. C. (2010) A continuous kinetic assay for adenylation enzyme activity and inhibition. *Anal. Biochem. 404*, 56–63.

(41) Bythrow, G. V., Mohandas, P., Guney, T., Standke, L. C., Germain, G. A., Lu, X., Ji, C., Levendosky, K., Chavadi, S. S., Tan, D. S., and Quadri, L. E. N. (2019) Kinetic Analyses of the Siderophore Biosynthesis Inhibitor Salicyl-AMS and Analogues as MbtA Inhibitors and Antimycobacterial Agents. *Biochemistry 58*, 833–847.

(42) Lux, M. C., Standke, L. C., and Tan, D. S. (2019) Targeting adenylate-forming enzymes with designed sulfonyladenosine inhibitors. *J. Antibiot. (Tokyo) 72*, 325–349.

(43) Ueda, H., Shoku, Y., Hayashi, N., Mitsunaga, J., In, Y., Doi, M., Inoue, M., and Ishida, T. (1991) X-ray crystallographic conformational study of 5′-O-[N-(l-alanyl)-sulfamoyl]adenosine, a substrate analogue for alanyl-tRNA synthetase. *Biochim. Biophys. Acta BBA - Protein Struct. Mol. Enzymol. 1080*, 126–134.

(44) Liu, F., and Austin, D. J. (2001) A General Synthesis of 5‘-Azido-5‘-deoxy-2‘,3‘- *O* -isopropylidene Nucleosides. *J. Org. Chem. 66*, 8643–8645.

(45) Dawadi, S., Kawamura, S., Rubenstein, A., Remmel, R., and Aldrich, C. C. (2016) Synthesis and Pharmacological Evaluation of Nucleoside Prodrugs Designed to Target Siderophore Biosynthesis in Mycobacterium tuberculosis. *Bioorg. Med. Chem. 24*, 1314–1321.

(46) Tipparaju, S. K., Joyasawal, S., Pieroni, M., Kaiser, M., Brun, R., and Kozikowski, A. P. (2008) In Pursuit of Natural Product Leads: Synthesis and Biological Evaluation of 2-[3-hydroxy-2-[(3-hydroxypyridine-2-carbonyl)amino]phenyl]benzoxazole-4-carboxylic acid (A-33853) and Its Analogues: Discovery of *N* -(2-Benzoxazol-2-ylphenyl)benzamides as Novel Antileishmanial Chemotypes. *J. Med. Chem. 51*, 7344–7347.

(47) Qiao, C., Wilson, D. J., Bennett, E. M., and Aldrich, C. C. (2007) A Mechanism-Based Aryl Carrier Protein/Thiolation Domain Affinity Probe. *J. Am. Chem. Soc. 129*, 6350–6351.

(48) Sundlov, J. A., Shi, C., Wilson, D. J., Aldrich, C. C., and Gulick, A. M. (2012) Structural and Functional Investigation of the Intermolecular Interaction between NRPS Adenylation and Carrier Protein Domains. *Chem. Biol. 19*, 188–198.

(49) Drake, E. J., Miller, B. R., Shi, C., Tarrasch, J. T., Sundlov, J. A., Leigh Allen, C., Skiniotis, G., Aldrich, C. C., and Gulick, A. M. (2016) Structures of two distinct conformations of holo-non-ribosomal peptide synthetases. *Nature 529*, 235–238.

(50) Miller, B. R., Drake, E. J., Shi, C., Aldrich, C. C., and Gulick, A. M. (2016) Structures of a Nonribosomal Peptide Synthetase Module Bound to MbtH-like Proteins Support a Highly Dynamic Domain Architecture. *J. Biol. Chem. 291*, 22559–22571.

(51) Reuter, D., McIntosh, J., Guinn, A., Madera, A. (2003) Synthesis of Vinyl Sulfonamides Using the Horner Reaction. *Synthesis 15*, 2321-2324.

(52) Gerratana, B. (2012) Biosynthesis, synthesis, and biological activities of pyrrolobenzodiazepines: Activities of Pyrrolobenzodiazepines. *Med. Res. Rev. 32*, 254–293.

(53) Mantaj, J., Jackson, P. J. M., Rahman, K. M., and Thurston, D. E. (2017) From Anthramycin to Pyrrolobenzodiazepine (PBD)-Containing Antibody–Drug Conjugates (ADCs). *Angew. Chem. Int. Ed. 56*, 462–488.

(54) Hertzberg, R. P., Hecht, S. M., Reynolds, V. L., Molineux, I. J., and Hurley, L. H. (1986) DNA sequence specificity of the pyrrolo[1,4]benzodiazepine antitumor antibiotics. Methidiumpropyl-EDTA-iron(II) footprinting analysis of DNA binding sites for anthramycin and related drugs. *Biochemistry 25*, 1249–1258.

(55) Hurley, L. H., Reck, T., Thurston, D. E., Langley, D. R., Holden, K. G., Hertzberg, R. P., Hoover, J. R. E., Gallagher, G., and Faucette, L. F. (1988) Pyrrolo[1,4]benzodiazepine antitumor antibiotics: relationship of DNA alkylation and sequence specificity to the biological activity of natural and synthetic compounds. *Chem. Res. Toxicol. 1*, 258–268.

(56) Antonow, D., Barata, T., Jenkins, T. C., Parkinson, G. N., Howard, P. W., Thurston, D. E., and Zloh, M. (2008) Solution Structure of a 2:1 C2-(2-Naphthyl) Pyrrolo[2,1- *c*][1,4]benzodiazepine DNA Adduct: Molecular Basis for Unexpectedly High DNA Helix Stabilization † ‡. *Biochemistry 47*, 11818–11829.

(57) Petrusek, R., Uhlenhopp, E., Duteau, N., and Hurley, L. (1982) Reaction of Anthramycin with DNA. *J. Biol. Chem. 257*, 6207–6216.

(58) Balbo, S., Turesky, R. J., and Villalta, P. W. (2014) DNA Adductomics. *Chem. Res. Toxicol. 27*, 356–366.

(59) Hu, Y., Phelan, V., Ntai, I., Farnet, C. M., Zazopoulos, E., and Bachmann, B. O. (2007) Benzodiazepine Biosynthesis in Streptomyces refuineus. *Chem. Biol. 14*, 691–701.

(60) Kung Sutherland, M. S., Walter, R. B., Jeffrey, S. C., Burke, P. J., Yu, C., Kostner, H., Stone, I., Ryan, M. C., Sussman, D., Lyon, R. P., Zeng, W., Harrington, K. H., Klussman, K., Westendorf, L., Meyer, D., Bernstein, I. D., Senter, P. D., Benjamin, D. R., Drachman, J. G., and McEarchern, J. A. (2013) SGN-CD33A: a novel CD33-targeting antibody–drug conjugate using a pyrrolobenzodiazepine dimer is active in models of drug-resistant AML. *Blood 122*, 1455–1463.

(61) Hartley, J. A., Spanswick, V. J., Brooks, N., Clingen, P. H., McHugh, P. J., Hochhauser, D., Pedley, R. B., Kelland, L. R., Alley, M. C., Schultz, R., Hollingshead, M. G., Schweikart, K. M., Tomaszewski, J. E., Sausville, E. A., Gregson, S. J., Howard, P. W., and Thurston, D. E. (2004) SJG-136 (NSC 694501), a Novel Rationally Designed DNA Minor Groove Interstrand Cross-Linking Agent with Potent and Broad Spectrum Antitumor Activity. Part 1: Cellular Pharmacology, In vitro and Initial In vivo Antitumor Activity. *Cancer Research 64*, 6693-6699.

(62) Morgensztern, D., Besse, B., Greillier, L., Santana-Davila, R., Ready, N., Hann, C. L., Glisson, B. S., Farago, A. F., Dowlati, A., Rudin, C. M., Le Moulec, S., Lally, S., Yalamanchili, S., Wolf, J., Govindan, R., and Carbone, D. P. (2019) Efficacy and Safety of Rovalpituzumab Tesirine in Third-Line and Beyond Patients with DLL3-Expressing, Relapsed/Refractory Small-Cell Lung Cancer: Results From the Phase II TRINITY Study. *Clin. Cancer Res. 25*, 6958–6966.

(63) von Tesmar, A., Hoffmann, M., Pippel, J., Fayad, A. A., Dausend-Werner, S., Bauer, A., Blankenfeldt, W., and Müller, R. (2017) Total Biosynthesis of the

Pyrrolo[4,2]benzodiazepine Scaffold Tomaymycin on an In Vitro Reconstituted NRPS System. *Cell Chem. Biol. 24*, 1216-1227.e8.

(64) Li, W., Khullar, A., Chou, S., Sacramo, A., and Gerratana, B. (2009) Biosynthesis of Sibiromycin, a Potent Antitumor Antibiotic. *Appl. Environ. Microbiol. 75*, 2869–2878.

(65) Giessen, T. W., Kraas, F. I., and Marahiel, M. A. (2011) A Four-Enzyme Pathway for 3,5-Dihydroxy-4-methylanthranilic Acid Formation and Incorporation into the Antitumor Antibiotic Sibiromycin. *Biochemistry 50*, 5680–5692.

(66) Sikora, A. L., Wilson, D. J., Aldrich, C. C., and Blanchard, J. S. (2010) Kinetic and Inhibition Studies of Dihydroxybenzoate-AMP Ligase from *Escherichia coli*. *Biochemistry 49*, 3648–3657.

(67) Wolff, H., and Bode, H. B. (2018) The benzodiazepine-like natural product tilivalline is produced by the entomopathogenic bacterium Xenorhabdus eapokensis. *PLOS ONE* (van Berkel, W. J. H., Ed.) *13*, e0194297.

(68) Wilson, D. J., Shi, C., Teitelbaum, A. M., Gulick, A. M., and Aldrich, C. C. (2013) Characterization of AusA: A Dimodular Nonribosomal Peptide Synthetase Responsible for the Production of Aureusimine Pyrazinones. *Biochemistry 52*, 926–937.

(69) Chhabra, A., Haque, A. S., Pal, R. K., Goyal, A., Rai, R., Joshi, S., Panjikar, S., Pasha, S., Sankaranarayanan, R., and Gokhale, R. S. (2012) Nonprocessive [2 + 2]e- off-loading reductase domains from mycobacterial nonribosomal peptide synthetases. *Proc. Natl. Acad. Sci. U. S. A. 109*, 5681–5686.

(70) Couch, R., O'Connor, S. E., Seidle, H., Walsh, C. T., and Parry, R. (2004) Characterization of CmaA, an Adenylation-Thiolation Didomain Enzyme Involved in the Biosynthesis of Coronatine. *J. Bacteriol. 186*, 35–42.

(71) Keating, T. A., Suo, Z., Ehmann, D. E., and Walsh, C. T. (2000) Selectivity of the Yersiniabactin Synthetase Adenylation Domain in the Two-Step Process of Amino Acid Activation and Transfer to a Holo-Carrier Protein Domain †. *Biochemistry 39*, 2297–2306.

(72) Guo, C.-J., Chang, F.-Y., Wyche, T. P., Backus, K. M., Acker, T. M., Funabashi, M., Taketani, M., Donia, M. S., Nayfach, S., Pollard, K. S., Craik, C. S., Cravatt, B. F., Clardy, J., Voigt, C. A., and Fischbach, M. A. (2017) Discovery of Reactive Microbiota-Derived Metabolites that Inhibit Host Proteases. *Cell 168*, 517-526.e18.

(73) Secor, P. R., Jennings, L. K., James, G. A., Kirker, K. R., Pulcini, E. deLancey, McInnerney, K., Gerlach, R., Livinghouse, T., Hilmer, J. K., Bothner, B., Fleckman, P., Olerud, J. E., and Stewart, P. S. (2012) Phevalin (aureusimine B)Production by Staphylococcus aureus Biofilm and Impacts on Human Keratinocyte Gene Expression. *PLoS ONE* (Sumby, P., Ed.) *7*, e40973.

(74) Roberts, A. B., Gu, X., Buffa, J. A., Hurd, A. G., Wang, Z., Zhu, W., Gupta, N., Skye, S. M., Cody, D. B., Levison, B. S., Barrington, W. T., Russell, M. W., Reed, J. M., Duzan, A., Lang, J. M., Fu, X., Li, L., Myers, A. J., Rachakonda, S., DiDonato, J. A., Brown, J. M., Gogonea, V., Lusis, A. J., Garcia-Garcia, J. C., and Hazen, S. L. (2018) Development of a gut microbe–targeted nonlethal therapeutic to inhibit thrombosis potential. *Nat. Med. 24*, 1407–1417.

(75) Pellock, S. J., Creekmore, B. C., Walton, W. G., Mehta, N., Biernat, K. A., Cesmat, A. P., Ariyarathna, Y., Dunn, Z. D., Li, B., Jin, J., James, L. I., and Redinbo, M. R. (2018) Gut Microbial β-Glucuronidase Inhibition via Catalytic Cycle Interception. *ACS Cent. Sci. 4*, 868–879.

(76) Rooks, M. G., Veiga, P., Reeves, A. Z., Lavoie, S., Yasuda, K., Asano, Y., Yoshihara, K., Michaud, M., Wardwell-Scott, L., Gallini, C. A., Glickman, J. N., Sudo, N., Huttenhower, C., Lesser, C. F., and Garrett, W. S. (2017) QseC inhibition as an antivirulence approach for colitis-associated bacteria. *Proc. Natl. Acad. Sci. 114*, 142–147.

(77) Ashley, E. A. (2016) Towards precision medicine. *Nat. Rev. Genet. 17*, 507–522.

(78) Brown, E. D., and Wright, G. D. (2016) Antibacterial drug discovery in the resistance era. *Nature 529*, 336–343.

(79) Dykens, J. A., Sullivan, S. G., and Stern, A. (1987) Oxidative reactivity of the tryptophan metabolites 3-hydroxyanthranilate, cinnabarinate, quinolinate and picolinate. *Biochem. Pharmacol. 36*, 211–217.

(80) Glaubiger, D., Kohn, K. W., and Charney, E. (1974) The Reaction of Anthramycin with DNA III. Properties of the Complex. *Biochim. Biophys. Acta BBA - Protein Struct. Mol. Enzymol. 361*, 303–311.

(81) Kopka, M. L., Goodsell, D. S., Baikalov, I., Grzeskowiak, K., Cascio, D., and Dickerson, R. E. Crystal Structure of a Covalent DNA-Drug Adduct: Anthramycin Bound to C-C-A-A-C-G-T-T-G-G and a Molecular Explanation of Specificity. *Biochemistry 33*, 13593–13610.

(82) Puvvada, M. S., Hartley, J. A., Jenkins, T. C., and Thurston, D. E. (1993) A quantitative assay to measure the relative DNA-binding affinity of pyrrolo[2,1-c][1,4]benzodiazepine (PBD) antitumour antibiotics based on the inhibition of restriction endonuclease *BamhI*. *Nucleic Acids Res. 21*, 3671–3675.

(83) Gregson, S. J., Howard, P. W., Hartley, J. A., Brooks, N. A., Adams, L. J., Jenkins, T. C., Kelland, L. R., and Thurston, D. E. (2001) Design, Synthesis, and Evaluation of a Novel Pyrrolobenzodiazepine DNA-Interactive Agent with Highly Efficient Cross-Linking Ability and Potent Cytotoxicity. *J. Med. Chem. 44*, 737–748.

(84) Smellie, M., Bose, D. S., Thompson, A. S., Jenkins, T. C., Hartley, J. A., and Thurston, D. E. (2003) Sequence-Selective Recognition of Duplex DNA through Covalent Interstrand Cross-Linking: Kinetic and Molecular Modeling Studies with Pyrrolobenzodiazepine Dimers †. *Biochemistry 42*, 8232–8239.

(85) Gregson, S. J., Howard, P. W., Gullick, D. R., Hamaguchi, A., Corcoran, K. E., Brooks, N. A., Hartley, J. A., Jenkins, T. C., Patel, S., Guille, M. J., and Thurston, D. E. (2004) Linker Length Modulates DNA Cross-Linking Reactivity and Cytotoxic Potency of C8/C8‘ Ether-Linked C2- *exo* -Unsaturated Pyrrolo[2,1- *c*][1,4]benzodiazepine (PBD) Dimers. *J. Med. Chem. 47*, 1161–1174.

(86) Wells, G., Martin, C. R. H., Howard, P. W., Sands, Z. A., Laughton, C. A., Tiberghien, A., Woo, C. K., Masterson, L. A., Stephenson, M. J., Hartley, J. A., Jenkins, T. C., Shnyder, S. D., Loadman, P. M., Waring, M. J., and Thurston, D. E. (2006) Design, Synthesis, and

Biophysical and Biological Evaluation of a Series of Pyrrolobenzodiazepine−Poly(*N* -methylpyrrole) Conjugates. *J. Med. Chem. 49*, 5442–5461.

(87) Rahman, K. M., James, C. H., Bui, T. T. T., Drake, A. F., and Thurston, D. E. (2011) Observation of a Single-Stranded DNA/Pyrrolobenzodiazepine Adduct. *J. Am. Chem. Soc. 133*, 19376–19385.

(88) Ma, Y., Khojasteh, S. C., Hop, C. E. C. A., Erickson, H. K., Polson, A., Pillow, T. H., Yu, S.-F., Wang, H., Dragovich, P. S., and Zhang, D. (2016) Antibody Drug Conjugates Differentiate Uptake and DNA Alkylation of Pyrrolobenzodiazepines in Tumors from Organs of Xenograft Mice. *Drug Metab. Dispos. 44*, 1958–1962.

(89) Quadri, L. E. N., Weinreb, P. H., Lei, M., Nakano, M. M., Zuber, P., and Walsh, C. T. (1998) Characterization of Sfp, a *Bacillus subtilis* Phosphopantetheinyl Transferase for Peptidyl Carrier Protein Domains in Peptide Synthetases †. *Biochemistry 37*, 1585–1595.

(90) Copeland, R. A. (2013) Evaluation of Enzyme Inhibitors in Drug Discovery: A Guide for Medicinal Chemists and Pharmacologists. John Wiley & Sons, Inc., Hoboken, NJ, USA.

(91) Conti, E. (1997) Structural basis for the activation of phenylalanine in the non-ribosomal biosynthesis of gramicidin S. *EMBO J. 16*, 4174–4183.

(92) Moriarty, N. W., Grosse-Kunstleve, R. W., and Adams, P. D. (2009) Electronic ligand builder and optimization workbench (eLBOW): A tool for ligand coordinate and restraint generation. *Acta Crystallogr. D Biol. Crystallogr. 65*, 1074–1080.

(93) Croll, T. I. (2018) *ISOLDE* : a physically realistic environment for model building into low-resolution electron-density maps. *Acta Crystallogr. Sect. Struct. Biol. 74*, 519–530.

(94) Wang, M., Yu, N., Chen, L., Villalta, P. W., Hochalter, J. B., and Hecht, S. S. (2006) Identification of an Acetaldehyde Adduct in Human Liver DNA and Quantitation as N^2 -Ethyldeoxyguanosine. *Chem. Res. Toxicol. 19*, 319–324.

(95) Wang, M., Cheng, G., Villalta, P. W., and Hecht, S. S. (2007) Development of Liquid Chromatography Electrospray Ionization Tandem Mass Spectrometry Methods for Analysis of DNA Adducts of Formaldehyde and Their Application to Rats Treated with *N* -Nitrosodimethylamine or 4-(Methylnitrosamino)-1-(3-pyridyl)-1-butanone. *Chem. Res. Toxicol. 20*, 1141–1148.

(96) Castro-Pichel, J., García-López, M. T., and De las Heras, F. G. (1987) A facile synthesis of ascamycin and related analogues. *Tetrahedron 43*, 383–389.

(97) Argüelles, A. J., Sun, S., Budaitis, B. G., and Nagorny, P. (2018) Design, Synthesis, and Application of Chiral C_2 -Symmetric Spiroketal-Containing Ligands in Transition-Metal Catalysis. *Angew. Chem. Int. Ed. 57*, 5325–5329.

(98) Mori, S., Aoyama, T., and Shioiri, T. (1986) New methods and reagents in organic synthesis. 65. A stereoselective synthesis of tilivalline. *Tetrahedron Lett. 27*, 6111–6114.

For Table of Contents Use Only